Fault systems in the offshore sector of the Campi Flegrei caldera (southern Italy): Implications for nested caldera structure, resurgent dome, and volcano-tectonic evolution

Jacopo Natale [a,*], Giovanni Camanni [a], Luigi Ferranti [a,b], Roberto Isaia [c], Marco Sacchi [d], Volkhard Spiess [e], Lena Steinmann [e], Stefano Vitale [a,c]

[a] Dipartimento di Scienze della Terra, dell'Ambiente e delle Risorse (DiSTAR), Universita` di Napoli Federico II, Italy
[b] Istituto Nazionale di Geofisica e Vulcanologia, Roma, Italy
[c] Istituto Nazionale di Geofisica e Vulcanologia, Osservatorio Vesuviano, Italy
[d] Istituto di Scienze Marine (ISMAR), Consiglio Nazionale delle Ricerche (CNR), Sezione di Napoli, Italy
[e] Faculty of Geosciences, University of Bremen, Germany

A B S T R A C T

The structure of a caldera may influence its activity, making its understanding crucial for hazard assessment. Here, we analysed high-resolution seismic profiles in the Campi Flegrei (southern Italy) offshore sector. We recognised two main fault systems, including those associated with the formation of the caldera and those affecting the resurgent dome. The former system comprises three broadly concentric fault zones (inner, medial and outer ring fault zones) depicting a nested caldera geometry. Considering the relations between faults and seismic units that represent the marine and volcaniclastic successions filling the caldera, all ring faults were formed during the Campanian Ignimbrite eruption (40 ka) and subsequently reactivated during the Neapolitan Yellow Tuff eruption (15 ka). In this last caldera-forming event, the inner and medial fault zones accommodated most of the collapse and were episodically reactivated during the younger volcano-tectonic activity. The second fault system occurs in the apical zone of the resurgent dome and comprises dominantly high-angle normal faults that are mainly related to the volcano-tectonic collapse that followed the Agnano-Monte Spina Plinian eruption (4.55 ka). Finally, we provide a volcano-tectonic evolutionary model of the last 40 kyr, considering the interplay among ring and dome faults activity, volcaniclastic sedimentation, ground deformation and sea-level changes.

1. Introduction

Calderas are morpho-structural depressions associated with large-volume volcanic eruptions (e.g., Cole et al., 2005; Branney and Acocella, 2015). Often, caldera structures may control the following volcanic activity and frequently host long-lived hydrothermal/geothermal systems. With many calderas worldwide located in densely inhabited regions (Newhall and Dzurisin, 1988), reconstructing their structures is of utmost importance for hazard assessment and improvement of volcano monitoring networks (Sparks et al., 2012). The Campi Flegrei (CF) caldera in southern Italy (Fig. 1a) is one of the most studied volcanoes worldwide due to its high urbanisation, making the volcanic risk very high (e.g., Charlton et al., 2020). The CF caldera structural architecture is still a matter of debate; however, most of the authors suggest the existence of a nested structure (Orsi et al., 1992; Acocella, 2008, 2010; Vitale and Isaia, 2014), mainly resulting from two caldera-forming eruptions: the Campanian Ignimbrite, at 40 ka (Giaccio et al., 2017) and the Neapolitan Yellow Tuff at 15 ka (Deino et al., 2004) eruptions.

The on-land caldera boundaries (Fig. 1a) have been inferred through the distribution of younger volcanic vents (Scarpati et al., 1993; Orsi et al., 1996), field observations (Vitale and Isaia, 2014), and exploration drilling (Rosi et al., 1983). Moreover, the caldera structure has been inferred by different geophysical investigations, including geoelectrical and magnetotelluric (Troiano et al., 2019; Siniscalchi et al., 2019), gravity (Florio et al., 1999; Capuano et al., 2013), magnetic (Secomandi et al., 2003) and seismic tomography (Zollo et al., 2003; Judenherc and Zollo, 2004; De Siena et al., 2018; Pepe et al., 2019) surveys. Furthermore, like several other calderas worldwide, both felsic (e.g., Rabaul, Papua New Guinea; Robertson and Kilburn, 2016; Nisyros, Greece; Tibaldi et al., 2008) and basaltic (e.g., Sierra Negra and Alcedo volcanoes Galapagos; Bell et al., 2021; Galetto et al., 2019, respectively), the CF caldera is characterized by post-caldera ground uplift and subsidence confined within its rims (e.g., Isaia et al., 2019; Bevilacqua et al., 2020; Natale et al., 2022).

Offshore, several works reconstructed the general structure and stratigraphy using seismic reflection datasets of variable quality and

* Corresponding author.
E-mail address: jacopo.natale@unina.it (J. Natale).

resolution (Pescatore et al., 1984; Fusi et al., 1991; Milia, 1998; Milia et al., 2000; Aiello et al., 2012, 2016; Sacchi et al., 2014, 2019; Steinmann et al., 2016, 2018; Natale et al., 2020, 2022). Recently, analyses of high-resolution seismic reflection profiles have provided detailed images of the submerged caldera sector, allowing to obtain a more detailed stratigraphic reconstruction and shedding light on the caldera evolution (Sacchi et al., 2014; Steinmann et al., 2016, 2018; Natale et al., 2022; Marino et al., 2022). However, an accurate characterisation of the offshore volcano-tectonic architecture is still lacking.

In this work, we analysed a multiscale set of high-to very high-resolution seismic reflection profiles acquired in the CF offshore in the last decades to better characterise the main fault zones and reconstruct the evolution of the caldera and the volcano-tectonic processes in the last 40 kyr. The detailed characterisation of the fault geometry, kinematics and age provided in this work yields important implications for understanding the caldera evolution, the connection between the surface and the deep magmatic-hydrothermal system, the geothermal potential (e.g., Rosi and Sbrana, 1987; Carlino et al., 2012), the source of the offshore seismicity (Orsi et al., 1999; Di Luccio et al., 2015), and improve the characterization of volcanic hazard (e.g., Selva et al., 2012; Bevilacqua et al., 2015, 2016, 2017; Neri et al., 2015).

2. Geological setting

2.1. Volcano-tectonic evolution

The CF caldera is located along the Tyrrhenian Sea margin of southern Italy (inset in Fig. 1a; Vitale and Ciarcia, 2013, 2018; Vitale

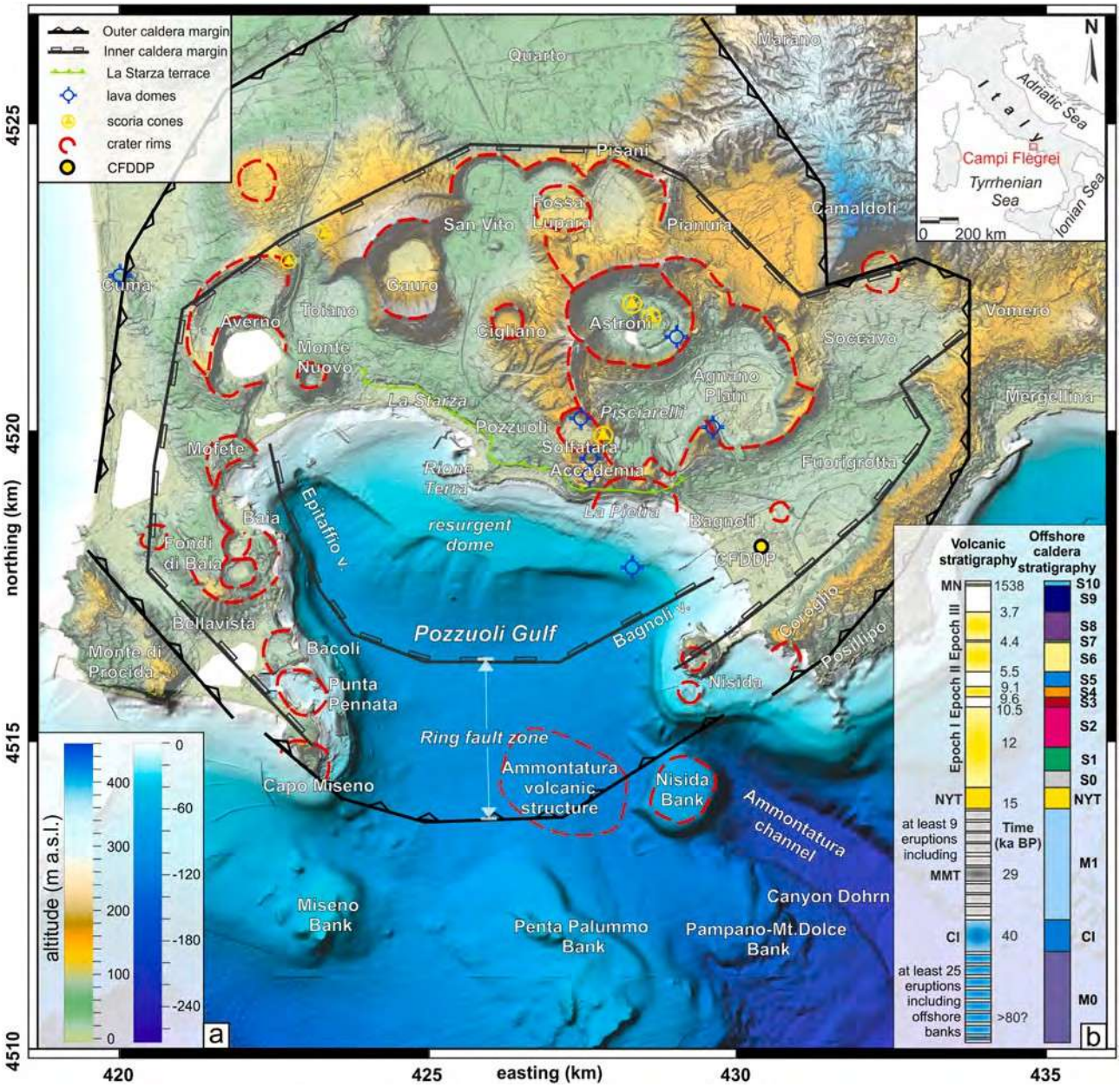

Fig. 1. (a) Digital Elevation Model of CF caldera, showing caldera and crater rims, scoria cone, and lava domes (after Isaia et al., 2018). Bathymetry is from Somma et al. (2016) and EMODnet Bathymetry Consortium (2018). CFDDP (De Natale et al., 2016) drill hole location is also indicated. (b) Simplified tephrostratigraphic logs of CF caldera in the last 80 kyr for the on-land and offshore (modified after Natale et al., 2022; Steinmann et al., 2016) Abbreviations: CI: Campanian Ignimbrite; MMT: Masseria del Monte Tuff; NYT: Neapolitan Yellow Tuff; MN: Monte Nuovo. (For interpretation of the references to colour in this figure legend, the reader is referred to the Web version of this article.)

et al., 2020 and reference therein). Volcanism in the CF caldera is older than 80 ka (Pappalardo et al., 1999), probably extending back to at least ~110 ka (Petrosino et al., 2019; Monaco et al., 2022), and was characterised by scattered volcanic activity with some volcanic edifices located in the urban area of Naples (Isaia et al., 2018). The CF area (Fig. 1a) hosted at least three large (>10 km^3 of erupted magma DRE, Dense Rock Equivalent) eruptions: the Campanian Ignimbrite (CI, 40 ka, up to 200 km^3 DRE, Costa et al., 2012; Giaccio et al., 2008, 2017; Scarpati and Perrotta, 2016, 2020; Silleni et al., 2020); the Masseria del Monte Tuff (MMT, 29.3 ka, 16 km^3 DRE; Albert et al., 2019) and the Neapolitan Yellow Tuff (NYT, 15 ka, 25–40 km^3 DRE, Orsi et al., 1992; Scarpati et al., 1993; Deino et al., 2004). Based on textural characteristics and the occurrence of an angular unconformity, the NYT has been divided into Lower (LM) and Upper (UM) members (Orsi et al., 1992).

The present morphological depression of the CF primarily derives from the younger NYT caldera collapse, partially masking the preexisting CI caldera (Orsi et al., 1996). Following the NYT event, mostly small-scale explosive volcanism occurred within and along the boundaries of the CF caldera, varying in style and magnitude (Bevilacqua et al., 2015, 2017). Eruptions occurred in closely spaced volcanic epochs, namely Epoch 1 (15-10.5 ka), Epoch 2 (9.6–9.1 ka), Epoch 3 (5.5–3.7 ka), lasting from centuries to millennia, alternated with periods of quiescence up to some millennia (e.g., Di Vito et al., 1999; Smith et al., 2011). The largest event during Epoch 1 and 2 has been the Pomici Principali Plinian eruption, which was followed by a subsidence phase (Natale et al., 2022). Epoch 3 has been further divided into 3a and 3b, with the occurrence of a rapid subsidence phase shortly after the Agnano-Monte Spina eruption (AMS, 4.55 ka; Smith et al., 2011), also marked by the deposition of the transgressive marine-transitional Pozzuoli Unit (Isaia et al., 2009, 2019).

Eruptions took place along the major structural discontinuities (Vitale and Isaia, 2014; Isaia et al., 2015; Bevilacqua et al., 2016) and have been coupled to significant ground deformation and seismo-tectonic activity, such as inferred by the widespread paleoliquefaction seismic-related structures hosted in the volcanic record (Vitale et al., 2019, 2022), which continues nowadays (Di Luccio et al., 2015; Young et al., 2020; De Martino et al., 2021; Giudicepietro et al., 2021; Isaia et al., 2021; Tramelli et al., 2022). In the long-term (~10 kyr), the caldera floor suffered a magmatic-related deformation (i.e., caldera resurgence), which resulted in a net uplift that led to the exposure of the marine-transitional sedimentary sequence of the La Starza Unit (Isaia et al., 2019; Vitale et al., 2019), presently cropping out along the Pozzuoli coast. Also, in the last 2000 years, the caldera floor was affected by alternating periods of uplift and subsidence, including a significant ground deformation associated with the historical eruption of Monte Nuovo (1538 CE; Guidoboni and Ciuccarelli, 2011; Di Vito et al., 2016; Amoruso et al., 2017). Similarly, ground movements occurred in the last ~50 years, showing pattern similarities with the long-term caldera floor movements (e.g., Del Gaudio et al., 2010).

2.2. Structural framework

According to Vitale and Isaia (2014), fault orientations within the CF caldera result from the interplay between the regional tectonic field and the local volcano-tectonic deformation. Structural studies in the CF caldera, both on-land (Isaia et al., 2015, 2021; Vitale and Isaia, 2014; Bevilacqua et al., 2020; Diamanti et al., 2022) and offshore (e.g., Natale et al., 2020), have documented the occurrence of faults associated with the activity of volcanic vents, caldera rims, and ground deformation (Fig. 1a). Generally, faults show a prevalence of regional tectonic trends (NW-SE and NE-SW). Nonetheless, ~N–S and ~E-W trending faults also occur in association with the youngest deformation episodes within the caldera (e.g., Vitale and Isaia, 2014; Vitale et al., 2019; Isaia et al., 2021). While older NW-SE and NE-SW faults show displacements up to tens of meters, younger faults exhibit metric displacements (e.g., Natale et al., 2020; Isaia et al., 2021). The central sector of the caldera is also characterised by intense degassing and hydrothermal activity (e.g., Chiodini et al., 2012; Cardellini et al., 2017; Young et al., 2020) and by the highest values of surface fractures and fault density, clustered around the town of Pozzuoli and in the Solfatara area (Bevilacqua et al., 2015, 2020). Fluid overpressure during the ongoing unrests triggers the reactivation of such faults, causing shallow seismicity felt by the population (e.g., D'Auria et al., 2011; Di Luccio et al., 2015; Isaia et al., 2021; Di Lieto et al., 2021; Tramelli et al., 2022).

2.3. The offshore sector of the CF caldera

The 6 × 7 km wide Pozzuoli Gulf hosts over one-third of the CF caldera. Its morphology results from the interaction between sea-level rise, ground deformation, erosion, and sedimentation and includes different features (Fig. 1a). The sector adjacent to the coastline has a truncated bell shape and represents the offshore part of the resurgent dome (e.g., Sacchi et al., 2014), which is the most prominent evidence of long-term ground deformation that caused the uplift of marine sediments of the La Starza Unit (Isaia et al., 2019; Natale et al., 2022 and references therein). The inner continental shelf develops on the submerged part of the dome at depths of 20–40 m b.s.l. The gulf reaches depths up to 120 m b.s.l. between Capo Miseno and Nisida Bank, in correspondence with the caldera ring fault zone (Fig. 1a). The latter is broadly 2.5 km wide and mainly composed of inward-dipping faults that displace the NYT unit and older rocks (Natale et al., 2022 and references therein). The southernmost faults have been associated with the CI caldera collapse (Fig. 1a; Steinmann et al., 2016) and confine the pre-CI volcanic highs in its footwall, including the Penta Palummo and Miseno banks (Fig. 1a).

The seismo-stratigraphic frame used in this work derives from the works of Steinmann et al. (2016) and Natale et al. (2022). The overall stratigraphy (Fig. 1b) constrains the relationships between the mapped faults and the caldera infill within the maximum penetration of seismic records (300–350 ms Two Way Time (TWT)). The imaged stratigraphic section (Fig. 1b) includes pre-CI rocks (>40 ka), CI (40 ka), pre-NYT (<40 ka and >15 ka), NYT (15 ka) and younger units (<15 ka). From the seafloor down to the depth of the NYT unit, we adopted the high-resolution stratigraphy of Natale et al. (2022), composed of eleven units, from S0 to S10 (Fig. 1b). According to the seismic facies, stacking pattern and stratal geometry, these units can be grouped in pre-doming (S0–S2) and syn-doming sequences (S3–S10), the latter further subdivided in uplift- (S3, S4, S7, S8, S10) and subsidence- (S5, S7, S9) dominated units (Natale et al., 2022). The age of these units includes the volcanic activity of Epochs 1, 2 and 3 (e.g., Smith et al., 2011). For the deeper seismic units, we rely on the stratigraphic framework of Steinmann et al. (2016). For the sake of clarity, we adopted the seismic unit names of Steinmann et al. (2016) for the post-CI deposits (M1 unit), including the buried volcanic bank herein called Ammontatura structure, which is interdigitated with the M1 unit, and the Monte Dolce-Pampano bank, in the southern part of the gulf (Sacchi et al., 2020). Campanian Ignimbrite is labelled as CI unit, and the pre-CI deposits are labelled as M0. Pre-CI volcanic banks are Miseno, and Penta Palummo (Fig. 1a), which have an inferred age of ~100 ka (e.g., Milia, 2010) and are coeval to the oldest tephras on land (Pappalardo et al., 1999; Scarpati et al., 2013).

3. Materials and methods

This work is based on two datasets of high-resolution seismic profiles, namely Seistec_2013 and GeoB08 (Fig. 2a), resulting in more than 150 analysed seismic profiles. The Seistec dataset was acquired using the uniboom IKB-Seistec profiler (Simpkin and Davis, 1993; Mosher and Simpkin, 1999; Sacchi et al., 2019) by ISMAR-CNR of Naples in 2013. With a very-high source frequency at 2 kHz, this single channel system is characterized by high maximum vertical resolution (0.2 m), whereas maximum seismic penetration is in the order of 100–150 ms Two Way

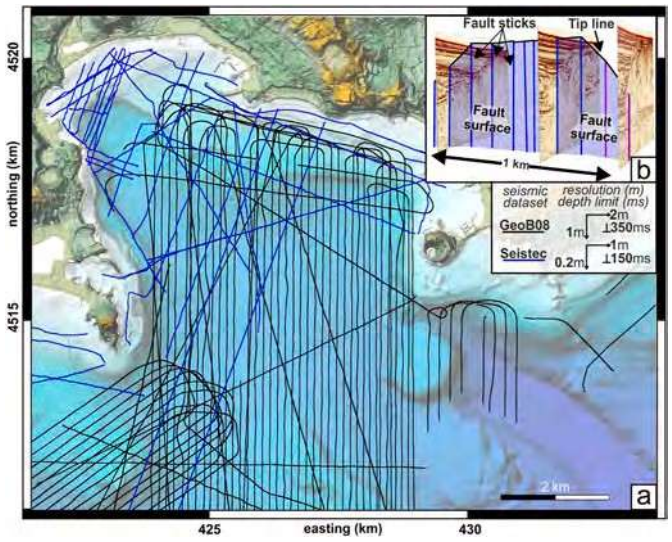

Fig. 2. (a) Location of seismic lines used in this work. Seismic penetration depth and spatial resolution are indicated for each dataset. (b) 3D oblique view of seismic profiles showing the fault sticks and interpolated fault surfaces.

Time (TWT).

To image the deeper reflectors and identify the NYT unit, we relied on the multichannel seismic lines from the GeoB08 dataset acquired during the CAFE-07 expedition in 2008 (Sacchi et al., 2009; Steinmann et al., 2016). The lower central source frequency of 250 Hz provides spatial resolution around 1–2 m with signal penetration exceeding 350 ms, with some local limitations due to fluid uprise blanking and shallow water seafloor multiple reflections (Steinmann et al., 2016).

Seismic lines were imported and analysed through Eliis Paleoscan software packages (Paleoscan, 2018). To estimate the thickness of seismic units and gather information on the dip angle of faults, we used a two-way time (TWT) velocity of 2000 m/s, which is representative of the whole investigated infill, made of mostly unconsolidated volcaniclastic deposits, tuffites and marine deposits (Sacchi et al., 2014; Steinmann et al., 2018; Natale et al., 2022), in agreement with the P-wave velocity in the first 2000 m, as deduced from seismic tomographic studies (Zollo et al., 2003; Vanorio et al., 2005).

The lines from the two datasets are mainly N–S oriented with some oblique lines and a few approximately E-W oriented tie lines that cover the central part of the Pozzuoli Gulf, with an average spacing of 150 m (Fig. 2a). Over 1200 fault sticks (2D fault traces) have been mapped in the whole dataset and then interpolated to reconstruct fault planes (Fig. 2b). Every fault segment has been interpolated by joining at least three fault sticks. The over 350 mapped fault planes were analysed and plotted with Open Stereo (Grohmann and Campanha, 2010) and TectonicsFP (Reiter and Acs, 1996–2022) open-source software to determine their average dip directions and dips.

The mapped fault planes obtained from the interpretation of seismic lines allowed us to construct a detailed structural map of the Pozzuoli Gulf and reconstruct the volcano-tectonic evolution of the area. However, fault mapping has some limitations, especially in the dome area, where individual fault planes have a limited length. In addition, the ~N–S-oriented faults in the same area might have been under-sampled due to the limited density of E-W trending seismic profiles. The main limitation for fault mapping in the deeper part of the gulf were acoustic blanking and relatively low signal penetration.

4. Results

4.1. Structural features of ring and dome faults

The N–S (Fig. 3a), NW-SE (Fig. 3b), and E-W (Fig. 3c) GeoB08 profiles illustrate the structural setting of the offshore CF caldera from the ring fault zone to the resurgent dome. In the northern part of the N–S trending GeoB08-042 profile (Fig. 3a), the resurgent dome is evident, with the stratal architecture documenting the several phases of caldera floor deformation described in Natale et al. (2022). The dome connects southward with the caldera collar, where the ring faults dislocate the NYT unit (Fig. 3a). Southward, the CI unit onlaps on the older volcanic bank of Penta Palummo, located in the extra-caldera area (Fig. 3a).

On the NW-SE trending GeoB08-102 line (Fig. 3b), the ~3 km wide resurgent dome fault zone is visible, with the high-angle faults dislocating the succession up to the S7 unit (~4.4 ka, Natale et al., 2022). The inner and the medial ring faults clearly dissect the NYT unit. The hanging wall of the inner ring hosts one of the several dikes mapped in the seismic profiles. The stratified southern end of the Nisida (NI) tuff cone covered by prograding clinoforms younger than 3.7 ka is also visible.

The NYT unit on the E-W trending GeoB08-026 line onlaps onto older marine and volcaniclastic units (M1 unit), including the 2 km wide Ammontatura structure (AMB, Fig. 1a; 3c), which in turn is interdigitated within this unit. The buried volcanic structure shows a gently northeastward-inclined abrasion surface truncating the underlying strata and is intensely affected by faults that locally convey uprising fluids, depicted by acoustic turbidity and high-amplitude, low-frequency reversed-phase reflections (Fig. 3c). The eastern termination of the Ammontatura volcanic structure (Fig. 3c) is overlain by the younger volcanic products of the Nisida bank (~12 ka, Natale et al., 2022), characterised by steeply inclined stratified flanks distinctive of tuff cones (Bischoff et al., 2021) and located at the erosive head of the Ammontatura channel (Fig. 1a; Aiello et al., 2020). On the western sector of the GeoB08-026 profile (Fig. 3c), the submarine portion of the well-stratified flanks of the Capo Miseno tuff cone and its eastern collapsed sector are covered by the prevalently transparent S9 unit that follows Epoch 3b (<3.7 ka, Natale et al., 2022). Underneath the Capo Miseno deposits, the upper part of the S2 unit increases in thickness westward. It corresponds to the southward continuation of the Porto Miseno tuff ring buried by the younger Capo Miseno tuff cone (Fig. 3b). The area east of the Capo Miseno tuff cone is deeply affected by fluid uprise that makes the seismic signal extremely turbid (Fig. 3c).

The main strands of the inner, medial, and outer ring fault zones are shown in Fig. 3d–f, which are also the sites of intense degassing (Fig. 3a–c). Although the throw on the inner and medial ring faults is locally variable, the NYT unit is averagely displaced by ~35–40 m (Fig. 3e). Although the S1 or S2 units seal most faults, some of them also cut upward into younger sequences (Fig. 3d and e).

Profiles across the resurgent dome document that this structure is pervasively affected by high-angle normal faults that form two main NE-SW structural low structures in the western part of the fault zone and three main NNE-SSW oriented west-dipping faults in the eastern sector. Unlike the ring fault systems, all of these faults cross-cut units younger than NYT (Fig. 4). These faults extend from the coast toward the southern part of the dome for ~2.7 km along strike. The line GeoB08-066, oriented E-W parallel to the coast (Fig. 4a), shows displacements exceeding 10 m and faults truncated by the abrasion surface associated with the S8 unit (<4.4 ka, Natale et al., 2022). The pervasive distribution of these faults is observable on the compound line GeoB08-048-49 (Fig. 4b) closer to the coastline, where the faults affect all the succession up to the abrasion surface. More to the south, line Seistec-801 (Fig. 4c) records the largest (~20 m) throw, whereas line GeoB08-065 (Fig. 4d) shows smaller throws along the strike of the western faults compared to the profiles more to the north. The N–S zoomed insets of GeoB08 lines show the NE-SW faults affecting the western part of the inner shelf (line GeoB08-028, in Fig. 4e) and the E-W faults located in the eastern part (line GeoB08-047, Fig. 4f).

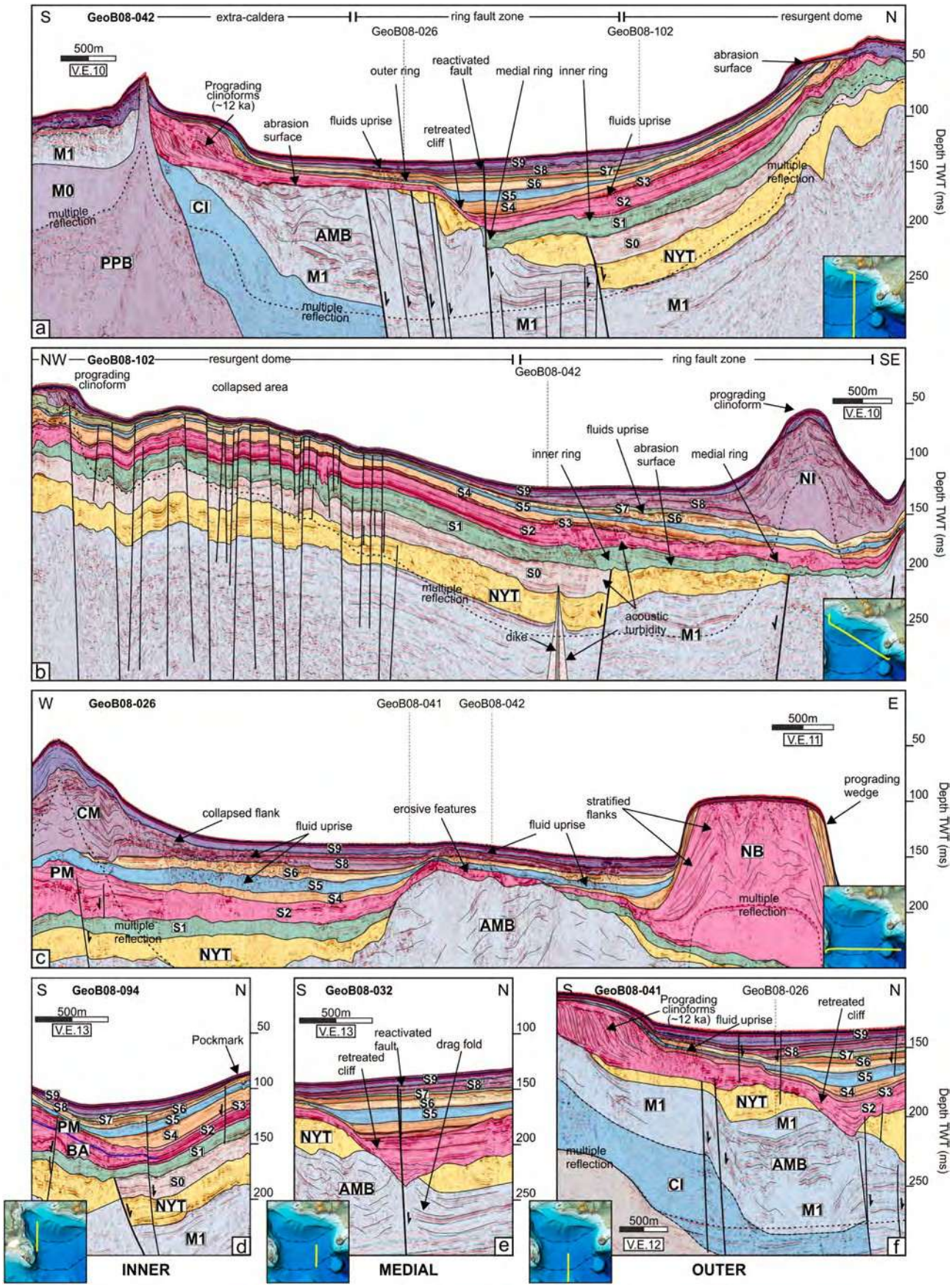

(caption on next page)

Fig. 3. (a) 8 km long N–S oriented GeoB08-042 seismic profile illustrating the main features of the caldera ring fault zone and the resurgent dome, including the several generations of depositional and erosive features. (b) 7 km long NW-SE oriented GeoB08-102 seismic profile showing the 2.5 km wide resurgent dome fault zone and the inner and medial ring faults. Dike intruded in the hanging wall of the inner ring fault is also indicated, as well as the submerged portion of the Nisida (NI) tuff cone. (c) 7 km long E-W oriented GeoB08-026 seismic profile showing the stratigraphic architecture of the caldera offshore, highlighting the stratigraphic position of different volcanic banks (Capo Miseno (CM) to the west, Ammontatura (AMB) to the south and Nisida Bank (NB) to the east). (d) N–S oriented zoomed section of GeoB08-094 seismic profile showing the reactivated inner ring fault zone. (e) Zoomed section of the N–S oriented GeoB08-032 seismic profile showing the reactivated medial ring fault zone. (f) Zoomed section of the N–S oriented GeoB08-041 seismic profile showing the stratal architecture along the outer ring fault zone. Abbreviations: PPB: Penta Palummo Bank; CI: Campanian Ignimbrite; AMB: Ammontatura volcanic structure; NYT: Neapolitan Yellow Tuff. Uninterpreted seismic lines are available in the supplementary material. (For interpretation of the references to colour in this figure legend, the reader is referred to the Web version of this article.)

4.2. Structural map of CF caldera offshore

4.2.1. Ring fault system

We grouped the ring faults into three broadly concentric structures (inner, medial, and outer), consisting of major and secondary faults (Fig. 5a). Overall, the principal segments of the three zones are averagely spaced 0.8 km apart. Each of the three ring fault zones displays a well-developed segmentation pattern, and several magmatic dikes also occur.

4.2.1.1. Inner ring fault system (IRFS). The IRFS is the innermost caldera fault zone identified offshore and can be traced from Bagnoli, to the east, to Baia, to the west (green faults in Fig. 5a). All the mapped IRFS faults show a normal dip-slip kinematics, with planes predominantly dipping toward the caldera centre and a few antithetic ones. These faults display E-W to NE-SW strikes towards the eastern part of Pozzuoli Gulf, whereas they exhibit E-W to NW-SE and subordinately N–S strikes in the western part of the gulf (Fig. 5a). Dip angles show values between 46° and 83°, with an average of 66° (Fig. 5b, f), with the lowermost dip angles recorded for E-W striking planes. These faults are highly segmented, and in several places, adjacent fault planes overlap, forming relay zones (*sensu* Camanni et al., 2019 and Roche et al., 2021), especially where the fault trends swing from E-W to NE-SW or NW-SE (Fig. 5a). The IRFS displaces the NYT unit with an average throw of 40 m (Fig. 3a), which is maintained roughly constant across the whole fault system. Locally, to the west, these faults cut the younger marine-volcaniclastic infill up to S6 unit (~4.5 ka, Fig. 3d, indicated in Fig. 5a). The morphological expression of these faults is evident in the bathymetry, where they control the trend of the Epitaffio and Bagnoli valleys (Figs. 1a and 5a), with the latter partially overprinted by the Nisida tuff cone (~3.7 ka, Natale et al., 2022). Other noteworthy features are seven magmatic dikes mapped mainly in the hanging wall of the IRFS that can be followed up to 750 m along strike. The seismic expression is characterised by planar sub-vertical reflection-free zones, with upward-bent reflectors on the lateral contacts. The dikes are frequently topped by acoustic turbidity and downward bending reflectors (Fig. 3b) and cross-cut the post-NYT infill locally up to the S6 unit, although failing to reach either current or former seafloor surfaces.

4.2.1.2. Medial ring fault system (MRFS). The MRFS extends from Nisida to Bacoli (red faults in Fig. 5a) and is characterised by faults mainly dipping toward the caldera centre and by minor synthetic and antithetic strands, with a prevailing E-W orientation (Fig. 5a, c). The medial ring faults show dip angles ranging between 46° and 80°, with an average of 68° (Fig. 5g). The MRFS is composed of one main fault segment marked by an E-W striking subsequent paleo valley that developed along the fault scarp, placing the NYT unit in lateral contact with the pre-NYT Ammontatura volcanic structure (Fig. 3a). Some minor antithetic segments are present in its hanging wall. Most of the MRFS is associated with relatively short fault segments. Fault segmentation is more frequent in the western part of the MRFS, where it is also associated with the development of a series of small graben broadly oriented WNW-ESE (Fig. 5a), located in the footwall of the main strand. A left-stepping relay zone links the E-W main strand with a NE-SW segment to the east of Nisida. Although clear cut-offs of the NYT unit are only locally observed, these faults generally displace NYT and older units with a throw comparable to that of the IRFS. The NYT unit shows thickness variation across the main fault strand of the MRFS (Fig. 3a). Erosion strongly altered the morphology of this fault, which is marked by a receding scarp (Fig. 3e). Along a ~1 km long portion of the main fault strand (indicated in Fig. 5a), the MRFS locally cuts younger strata, almost reaching the seabed (Fig. 3a, e). The fault-bounded intrusion of the Pennata structure, active since 10.5 ka (Natale et al., 2022; Fig. 5a) is confined between the footwall of the IRFS and above the main MRFS.

4.2.1.3. Outer ring fault system (ORFS). The ORFS runs from Posillipo to Capo Miseno (Figs. 1a and 5a) and represents the outermost caldera rim. The CI unit occurs in its footwall, in depositional contact above unit M0 (Figs. 1a and 3a, f). This feature is the only occurrence of the CI unit at shallow depth (<350 ms) in the seismic dataset within the Pozzuoli Gulf.

In the area facing the eastern cliff of Capo Miseno, roughly covering 4 km^2, the seismic signal is strongly altered by a massive fluid-related acoustic blanking (indicated in Fig. 5a and visible in Fig. 3c). We mapped over 50 fault segments belonging to the ORFS, mainly oriented E-W and NE-SW (Fig. 5d), predominantly dipping toward the caldera centre with dip angles ranging between 56° and 86° (Fig. 5h), with an average of 72°. Several short, E-W striking faults are present in the hanging wall of the ORFS, bounding elongated graben between the ORFS with the MRFS. Similarly, to the medial ring faults, these structures have no direct bathymetric expressions; however, the occurrence of well-developed prograding clinoforms surrounding the pre-CI volcanic banks suggests relative tectonic stability in the footwall of these ring faults (Figs. 3a and 5a). Unlike the IRFS and MRFS, none of the ORFS segments cut through sequences younger than NYT (Fig. 3f).

4.2.2. Dome fault system (DFS)

We mapped 170 individual fault segments in the resurgent dome area, grouped into ~ 50 main faults (Fig. 5a). These structures are mostly normal faults, with very few steep planes showing reverse kinematics. The DFS forms a NE-SW to NNE-SSW (Fig. 5e) trending structurally lowered zone, confined between two external structural highs (Figs. 4 and 5a) that project landward of two coastal reliefs, namely Rione Terra to the west and La Pietra/Accademia to the east (Figs. 1a and 5a). These faults have a morphobathymetric expression only southward of the shelf break, hosting channels that convey sediments to the base of the slope (Fig. 5a). As opposed to this, on the shelf, a gently east-dipping terrace conceals these faults that do not affect the seafloor (Fig. 4). In detail, three fault sets with NE-SW, NNE-SSW and E-W strike compose the DFS (Fig. 5e, i). The NE-SW faults mainly occur in the western part of the dome, forming two main lowered fault blocks bounded by sub-vertical normal faults (Fig. 4c). The NNE-SSW set is mainly located on the central-eastern part of the lowered area, on the slope sector, and shows broadly parallel west dipping synthetic structures. The fault throws range broadly between 5 and 10 m, with the highest values exceeding 20 m (Fig. 4d). Finally, the E-W faults affect the whole area (Fig. 4f and g), mainly down throwing toward the north and locally linking to the NE-SW faults, with 1–5 m of displacement. The mapped faults show dip angles between 65 and 88°, with an average of 82° (Fig. 5e, i). Fault lengths along the strike range from 250 m to over 4 km. Although with less extent, also the dome faults convey fluids toward the sea bottom.

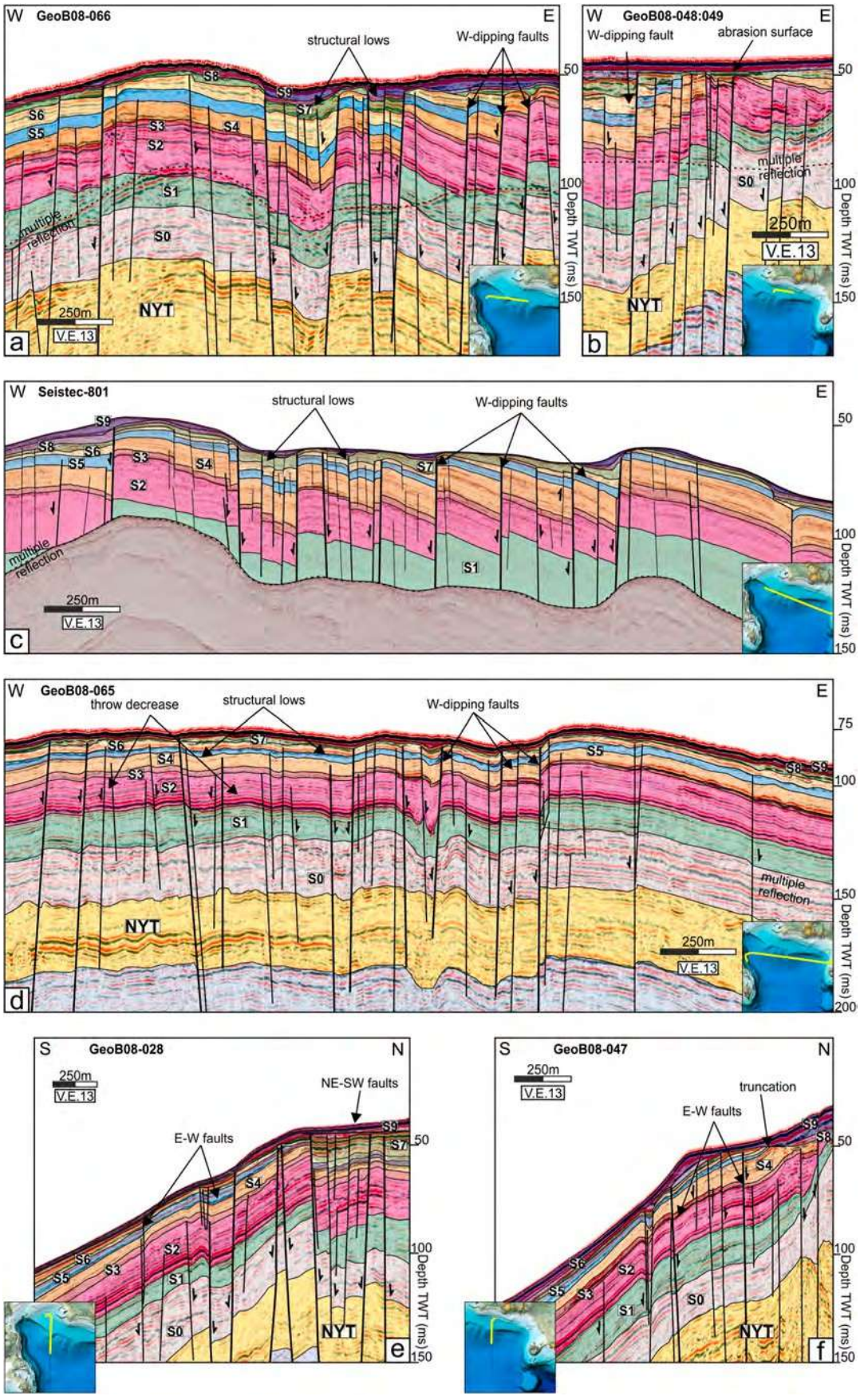

(caption on next page)

Fig. 4. E-W and N–S seismic sections show the collapse faults in the offshore part of the resurgent dome. (a) The E-W GeoB08-066 seismic profile displays the main faults arranged in a series of sub-parallel structural lows. (b) The E-W portion of two adjacent seismic profiles GeoB08-048-049 shows the distribution of faults tapped by the abrasion surface in the northeastern end of the dome fault zone (c). The E-W high-resolution Seistec-801 profile shows the different fault zone affecting the resurgent dome. (d) The E-W GeoB08-065 profile displays the southern end of the faults hosted in the dome. The decrease of throw of the individual fault zone is well evident. (e) The N–S GeoB08-028 profile shows E-W and the NE trending faults hosted in the western part of the shelf, highlighting the differences in the downthrow. (f) The N–S GeoB08-047 profile shows the E-W trending faults affecting the eastern part of the shelf. Abbreviations: NYT: Neapolitan Yellow Tuff. For profile location, see the bottom map inset. Uninterpreted seismic lines are available in the supplementary material.

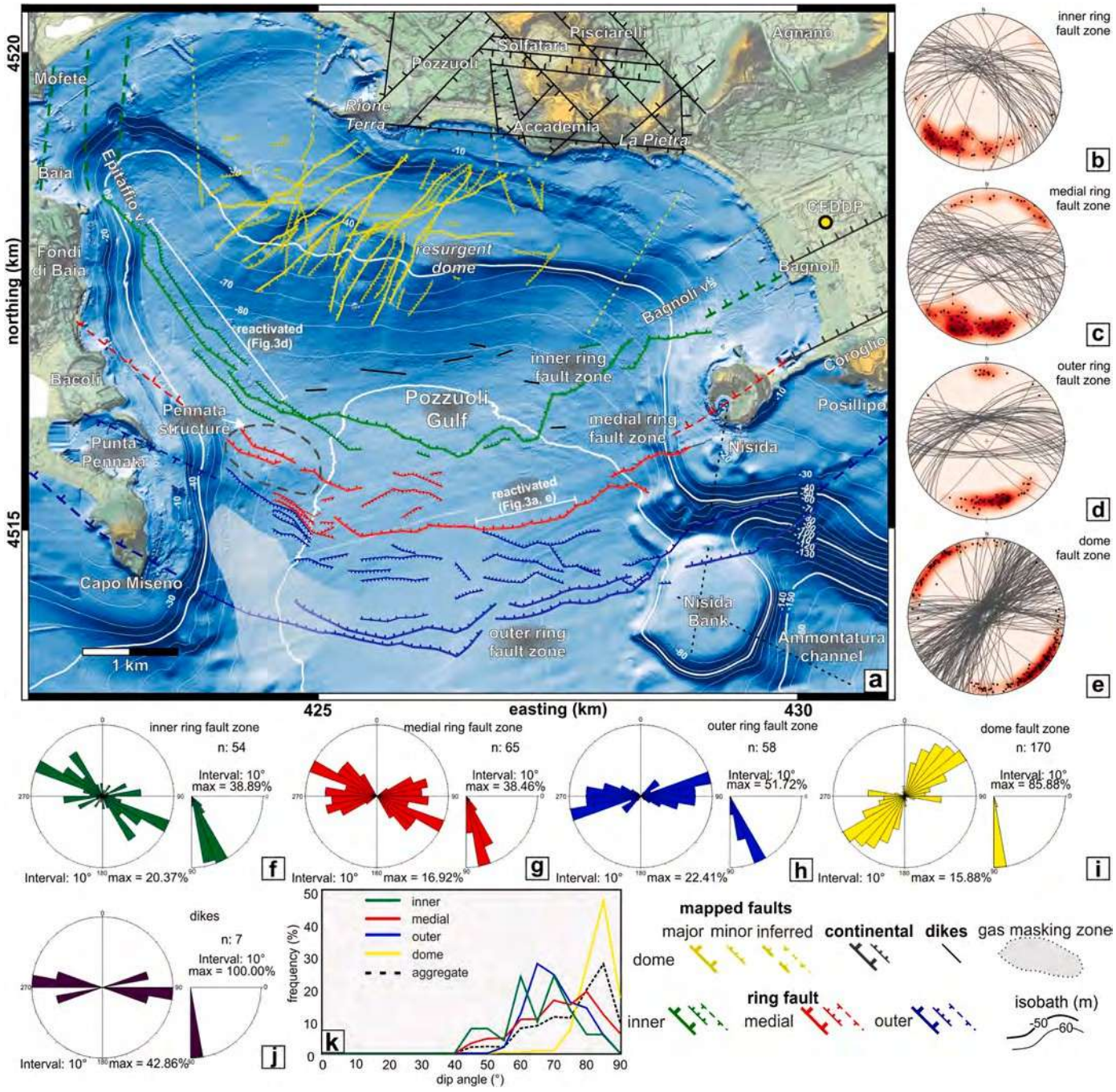

Fig. 5. (a) Structural map of the Campi Flegrei caldera offshore sector (Pozzuoli Gulf). Faults are colour-coded according to the legend and structural plots. Barbs indicate the downthrown block. Isobath contour interval is 10m (thin white lines), major contour interval is 50 m (thick white lines). Stereographic projections of mapped faults (equiareal net, lower hemisphere) (b) inner ring faults; (c) medial ring faults; (d) outer ring faults; (e) dome faults. Rose diagrams of fault strike and dip angle. (f) inner ring fault; (g) medial ring fault; (h) outer ring fault; (i) dome faults; (j) dikes; (k) dip angle frequency plot of the mapped faults. Projection of Pennata structure is after Natale et al. (2022). (For interpretation of the references to colour in this figure legend, the reader is referred to the Web version of this article.)

5. Discussion

In the following section, we address the evolution of the caldera structure and the dome fault system in relation to available information for the structures outcropping on land. Finally, we summarise the evolution of the offshore Campi Flegrei caldera during the different volcano-tectonic phases that have occurred in the last 40 kyr.

5.1. Offshore caldera structure

The existence and the origin of the Campi Flegrei caldera have been extensively debated in the literature, with some authors attributing the formation of the caldera to the CI eruption (i.a., Rosi and Sbrana, 1987; Sbrana et al., 2021), to the NYT eruption (Rolandi et al., 2003, 2020), or the combination of both (Orsi et al., 1996; Acocella, 2008, 2010; Vitale and Isaia, 2014). Here, we document that the caldera ring faults acted during two distinct collapse episodes, with the CI and the NYT caldera-forming eruptions, giving rise to a nested and telescopic depression.

In the seismic dataset, the CI unit is not recognised in the hanging wall of ORFS. On the contrary, it is observed at ~100 m b.s.l. in the extra-caldera areas, in stratigraphic contact with the pre-CI volcanic banks (Fig. 3a), similarly to what occurs on-land (Camaldoli, Quarto, and Monte di Procida; Fig. 1a; Di Girolamo et al., 1984; Rosi and Sbrana, 1987; Orsi et al., 1996; Vitale and Isaia, 2014). However, inside the caldera, the CI unit is not visible within the seismic penetration limit, i.e., ~350 ms (~300–350 m). This observation is consistent with the ~450–500 m (b.s.l.) depth at which CI occurs in the CFDDP (Campi Flegrei Deep Drilling Project) pilot borehole (Figs. 1, 5a and 6a; De Natale et al., 2016).

Furthermore, the depth of the NYT unit between ~200 and 250 m in the CFDDP borehole (Fig. 6a) is comparable to the ~200 m depth measured in the analysed seismic dataset in the hanging wall of the IRFS. The similar measured depths of NYT and inferred depths of CI in the Pozzuoli Gulf and the CFDDP suggest that also this borehole is located in the hanging wall of the westernmost caldera fault beneath the Bagnoli plain (i.e., the IRFS), in agreement with the borehole data of Calderoni and Russo (1998). Considering the aggregate downthrow along the three ring fault zones of both the CI and the NYT, the minimum collapse estimate is ~300–350 m (Fig. 6a). Subtracting the values of 100–120 m, summing the throw on the inner and the medial achieved during the NYT collapse (Fig. 6b), by difference the resulting 200–250 m value can be referred to the older CI caldera collapse (Fig. 6c), which records displacements along the caldera rims 2–3 times larger than that reconstructed for the NYT. This evaluation rules out the possible but less significant local collapses due to minor eruptions or tectonic activity and highlights that the caldera collapses granted the accommodation space for the subsequent emplacement of volcaniclastic and sedimentary deposits (M1 unit; Fig. 6b), while the effect of sea-level changes on accommodation space compared to the CI caldera formation is negligible.

This displacement estimate highlights that the caldera structure was already present during the NYT collapse, which reactivated the major fault planes, in agreement with previous works (Orsi et al., 1996; Acocella, 2008; Vitale and Isaia, 2014) and different from others (i.a., Rosi and Sbrana, 1987; Sbrana et al., 2021).

With the NYT unit well within the seismic penetration limit (s.p.l.), we could go into detail about the NYT collapse process offshore. The constant thickness of the NYT unit on both sides of the IRFS (Fig. 3a) suggests no syn-depositional faulting but a collapse toward the end of the eruption, as suggested by Wohletz et al. (1995) on land. In contrast, we observe thickness differences of the NYT unit between the MRFS hanging wall and footwall (Fig. 7c), albeit some uncertainty exists due to possible post-caldera erosion (Fig. 3a, b, d). This change in thickness might be linked to syn-depositional faulting of the NYT, similarly to what has been observed on the Coroglio cliff (Fig. 5a) by Scarpati et al. (1993) and Wohletz et al. (1995), who envisaged the start of the collapse during the early stages of emplacement of the NYT Upper Member, denoted by the emplacement of a lithic breccia and welded scoriae units. This feature suggests that the collapse progressed inward from the MRFS to the IRFS. Although being less evident (Fig. 7e), the ORFS likely reactivated during the NYT collapse, as suggested by the several faults affecting the Ammontatura structure, which conversely do not displace the gently inclined abrasion surface (Figs. 3a and 7c), in turn, sealed by the S2 unit (>12 ka, Natale et al. (2022) The activation of such peripheral faults is also described on land (Acocella, 2008; Vitale and Isaia, 2014).

These observations support the nested caldera model proposed by different authors (Orsi et al., 1996, 1999; Acocella, 2008; Vitale and Isaia, 2014). In such a scenario, the mapped outermost (ORFS) offshore caldera rim connects to Posillipo hill to the east and beneath Capo Miseno to the west, representing the outermost structural highs (Fig. 5a) of both caldera collapses. The innermost rim (IRFS) continues in the

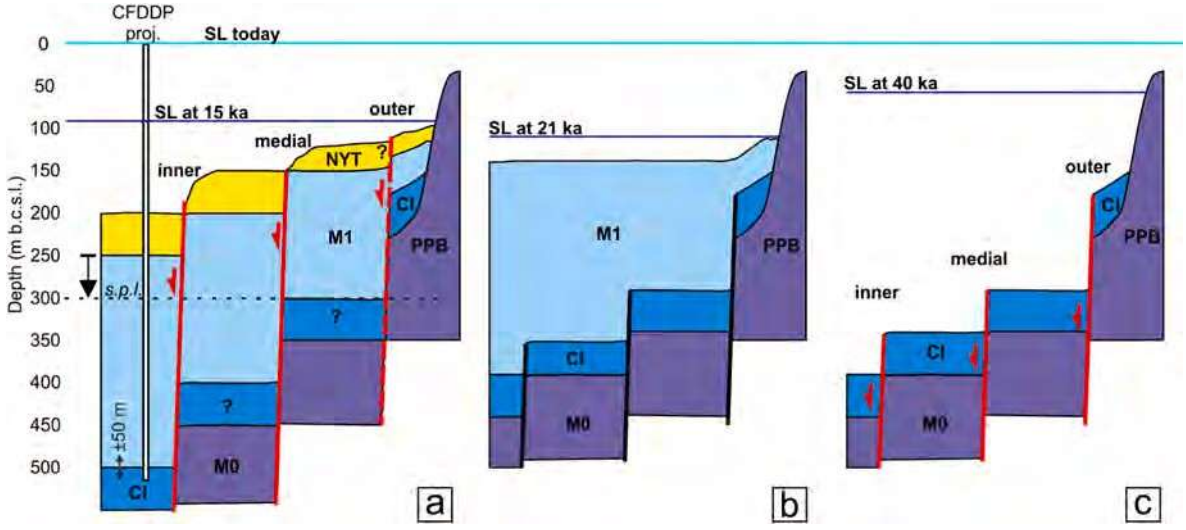

Fig. 6. (a–c) Schematic back-stripping cartoon summarising the ring fault zone evolution in the last 40 kyr. The constraint on unit depths results from seismic profiles and the CFDDP borehole, (location is in Figs. 1a and 5a). Abbreviations: S.p.l.: Seismic penetration limit. M0: Marine and volcaniclastic units older than CI. PPB: Penta Palummo Bank; CI: Campanian Ignimbrite; M1: Marine and volcaniclastic units younger than CI. NYT: Neapolitan Yellow Tuff. (For interpretation of the references to colour in this figure legend, the reader is referred to the Web version of this article.)

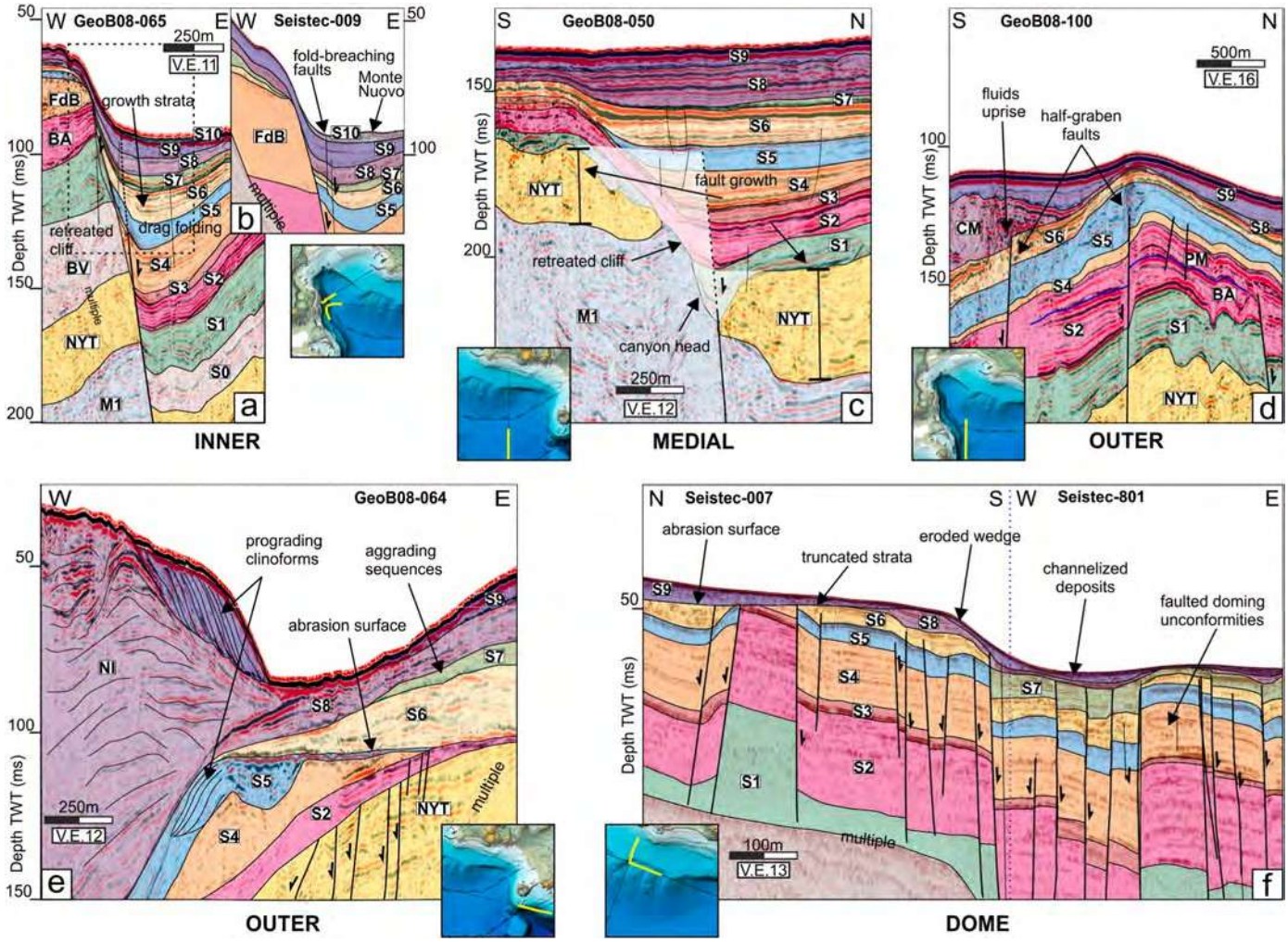

Fig. 7. Zoomed sections of selected fault zones. (a) The GeoB08-065 E-W profile shows the structural relationships between the hanging wall and the footwall of the western inner ring fault, highlighting the fault growth and drag folding of reflectors. (b) Zoomed section Seistec-009 with a high-resolution image of fault activity. (c) The GeoB08-050 N–S profile highlights the erosive features affecting the medial ring fault and thickness differences between hanging wall and footwall. (d) The GeoB08-100 N–S profile shows the uplifted Pennata structure and the graben faults affecting the S6 unit. (e) The E-W oriented GeoB08-064 shows the complex stratal architecture of the eastern outer ring fault system. (f) Compound profiles of high-resolution Seistec 007 (N–S) and 801 (E–W) show the relationships between faults, abrasion surface, and channelised deposits. Abbreviations: M1 Marine and volcaniclastic units younger than CI; NYT: Neapolitan Yellow Tuff; BV: Bellavista; BA: Bacoli; FdB; Fondi di Baia; CM; Capo Miseno; NI: Nisida. Uninterpreted seismic lines are available in the supplementary material.

Bagnoli plain to the east and along the Epitaffio-Averno alignment to the west (Figs. 1a and 5a).

This work clearly highlights the presence of an offshore caldera structure, in agreement with most of the previous literature, including geophysical data (Florio et al., 1999; Secomandi et al., 2003; Zollo et al., 2003; Capuano et al., 2013), and sensibly differently from studies that insist on denying the existence of the caldera (e.g., Torrente et al., 2010; Torrente and Milia, 2018 and references therein). However, compared to existing CF caldera structural models (e.g., Orsi et al., 1999; Acocella, 2008; Sbrana et al., 2021), our results bring elements of novelty, especially in terms of geometry and fault kinematics. For the first time, we mapped three distinct caldera rims instead of two caldera rims (Acocella, 2008; Sacchi et al., 2014; Steinmann et al., 2016, 2018) and depicted a sub-circular nested caldera structure differently from previous works that suggested a broader geometry running to the southeast including part of the gulf and the urban area of Naples and exposed pre-caldera deposits (Orsi et al., 1999; Perrotta et al., 2006).

We also underline that the surficial structures (<300 m) of the caldera rims in the offshore show moderate dip angles (~65°) with normal kinematics (Fig. 5k), differently from the previous literature that implied vertical faults (e.g., Orsi et al., 1996), or outward-dipping reverse faults such as predicted by analogue modelling at shallow levels (Acocella, 2008). However, the reverse faults may occur at deeper levels (below seismic penetration limit) to accommodate the horizontal movement triggered by the lithostatic collapse (e.g., Acocella, 2007) unless a significant extensional field occurs (Geyer and Martí, 2014). More importantly, despite the long-term caldera resurgence exceeding 100 m of in the last 15 kyr, no evidence of positive inversion (from normal to reverse kinematics) is found along the offshore ring faults, unlike the results of analogue models (e.g., Acocella et al., 2000), and seismic profiles interpretation (e.g., Corradino et al., 2021).

Some sectors of each ring fault system show evidence of deformation younger than the NYT collapse, which is here interpreted as due to the reactivation of preexisting faults. For the IRFS, most of the reactivation occurs in the western sector, both as faulting (Fig. 3c) or passive folding in the ~N–S segment near Bacoli and Baia (Fig. 7a and b), which results in hanging wall sequences thickening (i.e., growth strata) within seismic units younger than S3, as observed in other setting and experiments for blind normal faults (Hardy, 2011, 2013). This evidence suggests that normal fault motion is coupled with intra-caldera resurgence, allowing thicker sequences to be laid down in this part of the caldera collar (Fig. 7b). Furthermore, the MRFS cuts through units younger than NYT

(Fig. 3e), being reactivated during the early Epoch 3b (4.4–3.7 ka, Natale et al., 2022). Some antithetic fault arrays of the ORFS dislocate seismic reflectors up to S6–S7 unit but are sealed by the Capo Miseno tephra (~3.7 ka, S8 unit, Fig. 7d); these NW-SE striking, SW-dipping normal faults are also found on the coast, cutting the tuff of Bacoli volcano (Fig. 1a, S2 unit), and more to the west, affecting the tuffs of Torre Cappella and Bellavista (Isaia et al., 2018).

It was previously noticed (e.g., Steinmann et al., 2016) that an extensive fluid uprise occurs on the ring faults, which, together with the occurrence of dikes and sills (e.g., Punta Pennata bysmalith; Natale et al., 2022) emplacement along the ring fault system, suggests that the ring faults are preferred paths for the magmatic-hydrothermal fluid migration toward the surface, and significantly contribute to the gas output budget of the hydrothermal system. In concert with the matching between the mapped ring faults and the hydrothermally altered regions within the caldera (Walter, 2008), as marked by geophysical (Barberi et al., 1991; Corrado et al., 1998; Carlino et al., 2012; Jasim et al., 2015) and hydrogeochemical studies (e.g., Ebrahimi et al., 2022).

5.2. Dome faults

Several authors have mapped faults in the resurgent dome area using seismic reflection profiles (Colantoni et al., 1972; Sacchi et al., 2014; Natale et al., 2020; Corradino et al., 2021), while others (e.g., Orsi et al., 1999) have inferred them using the earthquake hypocentre distribution during the 1982-84 seismo-volcanic crisis. Based on solid geological observations, we provide a detailed geometric characterisation and a novel interpretation of the processes leading to forming such a fault system. In terms of geometry, we depict the coexistence of ~NE-SW and E-W faults in this area, with the ~NE-SW faults extending beneath the shelf toward the coast. Concerning the formation process of such a fault array, we exclude that this fault system can be related to the outer arc extension of the resurgent dome suggested by different authors (e.g., Corradino et al., 2021 and references therein). Our interpretation bases on the following factors: (i) faults are sub-vertical, implying negligible layer-parallel extension; (ii) lack of growth strata and multiple abrasion surfaces; and (iii) the last faulted units observed in the seismic profiles (Fig. 4; S6 and S7 units, ~4.4 ka, Natale et al., 2022) are covered by valley-ponding deposits of S8 unit (<4.3 ka), deposited during the Epoch 3b, well recorded in the offshore by a wide abrasion surface developed during the uplift phase (Fig. 7f). On land, recent works have reported faults cutting the equivalent of S6 unit (i.e., AMS tephra) and sealed by a paleosol (Vitale and Isaia, 2014; Isaia et al., 2019; Vitale et al., 2019; Bevilacqua et al., 2020). In addition, no evidence of fault reactivation exists in the offshore associated with the 15 m of uplift predating the Monte Nuovo eruption (Di Vito et al., 2016). The occurrence of almost vertical faults and the concurrency of normal and reverse kinematics are consistent with analogue models (Ruch et al., 2012) and field examples (Diamanti et al., 2022) of collapse faults that justify the recorded high throws. Likely, the two main sets of NE-SW and E-W faults mutually connect, producing hard-linked polygonal arrays (*sensu* Cartwright et al., 2003), suggesting a non-coherent collapse (i.e., piecemeal; Roche and Druitt, 2001). We suggest that the dome fault array is most likely associated with a single collapse episode, concurrent to the magma chamber emptying of the large-volume AMS eruption (>1 km^3 DRE; Di Vito et al., 1999; De Vita et al., 1999; Smith et al., 2011). This important event was also marked by the deposition of the transgressive Pozzuoli Unit separating Epoch 3a and 3b tephras (Isaia et al., 2009, 2019; Vitale et al., 2019; Natale et al., 2022). The activation of some faults associated with the Pomici Principali Plinian eruption (12 ka) cannot be ruled out, as its deformation resembles a similar pattern to AMS.

All this supports the reactivation of old inherited sub-vertical tectonic structures during discrete volcano-tectonic collapse (Vitale and Isaia, 2014). Furthermore, the mapped structures fit well with the known structures along the central coastal sector of the caldera, extending the uprise of hydrothermal fluids in the offshore part of the resurgent dome (Carlino et al., 2016).

5.3. Volcano-tectonic evolution in the last 40 kyr

The results of the present work have implications for the offshore evolution of the shallow structure of the CF caldera, as depicted in eight discrete stages from the formation of the CI caldera to the last historical eruption of Monte Nuovo (Fig. 8).

5.3.1. Stage1: Campanian Ignimbrite collapse

At ~40 ka, the CI collapse occurred (Fig. 8a), limiting the exposure of older rocks only on structural highs outside the caldera, including the volcanic banks of Penta Palummo and Miseno in the offshore. On land, these older rocks are represented by the Monte di Procida and Acquamorta volcanoes, Torregaveta lava, Punta Marmolite and Cuma lava domes and tephras, pre-CI rocks exposed at Camaldoli, and the tuff cones and rings cropping out in the urban area of Naples (Isaia et al., 2018).

5.3.2. Stage2: Intercaldera period

Following the CI eruption, the ORFS controlled the location of most of the post-CI vents, mainly placed within the collapsed area (Fig. 8b), except for the Pampano-Mt. Dolce bank (Sacchi et al., 2020) and the small mushroom-shaped volcanic unit recognised by Steinmann et al. (2016). In this time frame, also the eruption of Solchiaro at Procida occurred, representing an occurrence of tectonic-controlled off-caldera volcanic activity after the CI eruption (De Astis et al., 2004). The post-CI vents encompass the Torregaveta volcano, the Trentaremi tuff cone, and the Ammontatura buried bank. Other inter-caldera eruptions are reported in the literature, such as the Monterusciello, Verdolino, Masseria del Monte, Monticelli and Lagno Amendolare eruptions (Isaia et al., 2018). The extensional regional tectonics in this period could play an important role in localizing off-caldera volcanism.

5.3.3. Stage3: Neapolitan Yellow Tuff collapse

The NYT collapse occurred by partially reactivating the CI ring faults, firstly the MRFS and later the IRFS and subordinately the ORFS (Fig. 8c). The involvement of preexisting caldera structures seems crucial in collapse progression and also affected the tapping of different magma batches throughout the eruption (Forni et al., 2018). Compared to the CI collapse, the amount of displacement on the offshore structures was about three times smaller, in agreement with the different magnitude of the two eruptions.

5.3.4. Stage4: pre-doming post-NYT activity

Shortly after the NYT eruption, the volcanic activity clustered on the ring faults (Di Vito et al., 1999; Orsi et al., 2004; Bevilacqua et al., 2016). The Pomici Principali Plinian eruption was followed by marked subsidence (Natale et al., 2022), which was likely accompanied by the activity of normal faults in the coastal sector, creating accommodation space to host the marine-transitional units of La Starza (Fig. 8d).

5.3.5. Stage5: syn-doming post-NYT activity

The caldera resurgence that occurred during Epochs 2 and 3a (i.a., Isaia et al., 2019; Natale et al., 2022) was confined within the IRFS (Bevilacqua et al., 2020), whereas volcanism at this stage occurred between the IRFS and the MRFS (Fig. 8e). This doming phase inverted the previously formed depocenter of the caldera, producing ~60-80-m of uplift (Isaia et al., 2019; Natale et al., 2022), lasting until the AMS eruption. Coeval with this uplift phase, the western IRFS show evidence of reactivation.

5.3.6. Stage6: AMS collapse and Pozzuoli Unit deposition

The AMS eruption (4.55 ka) caused the formation of a minor caldera (Agnano Plain, Fig. 1a; 8f) but also the collapse of the central sector of the resurgent dome accommodated by the dome faults (Figs. 5a and 8f).

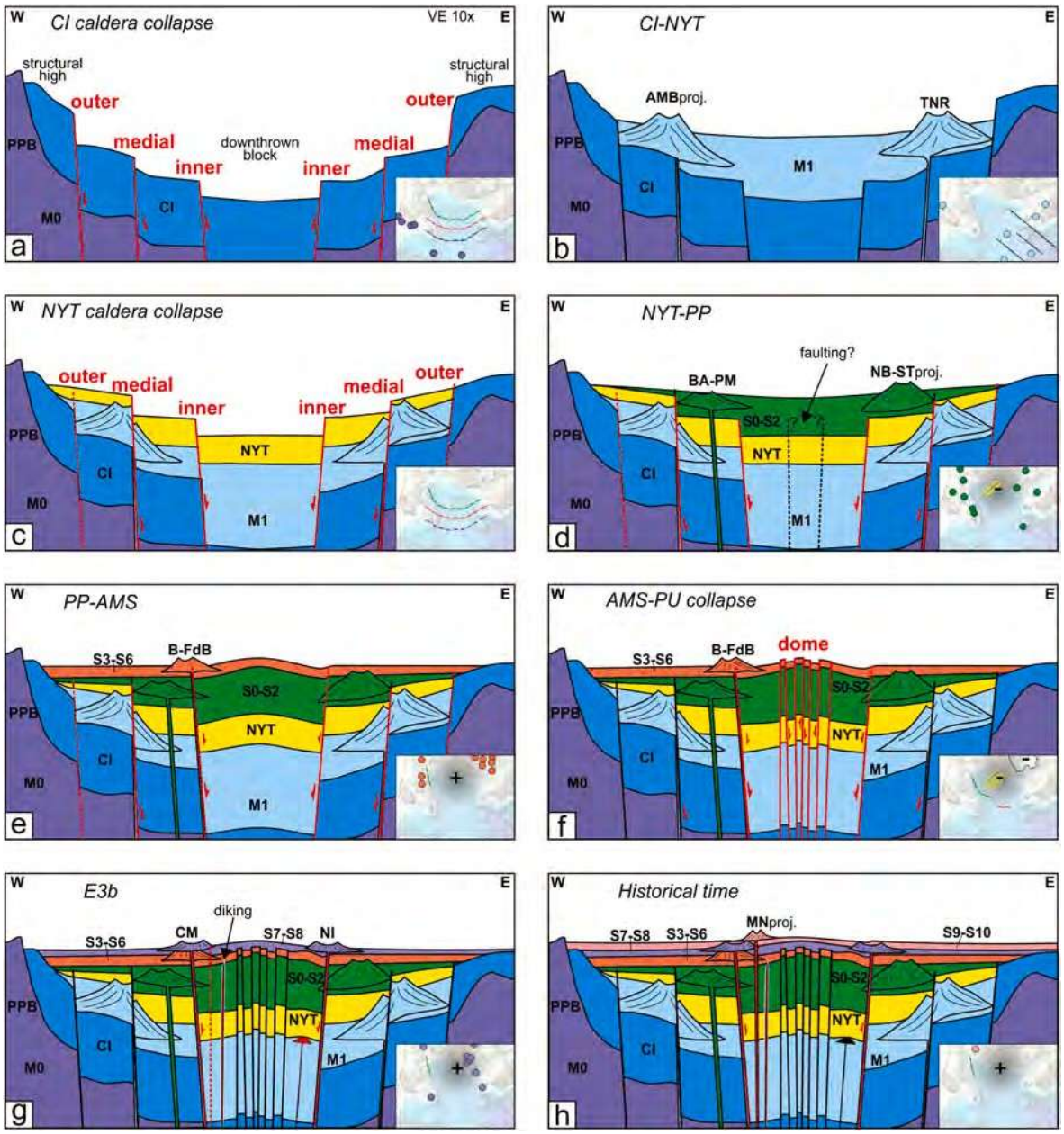

Fig. 8. E-W oriented cartoon sections summarising the evolution of the offshore sector of the CF caldera in the last 40 kyr. (a) CI caldera collapse, the map inset shows activated ring faults and older volcanic centres. (b) Sedimentation of M1 unit and post-caldera volcanism broadly focused on the caldera rims. (c) NYT caldera syn-eruptive collapse on MRFS and late collapse on IRFS. Map inset shows activated ring faults. (d) Post-NYT Epoch 1 volcanism and post-PP subsidence; map inset shows numerous eruptions along the peripheral zone. (e) Epoch 2 and 3a uplift centred in Pozzuoli associated with eruptions at the resurgent dome periphery. Map inset also shows the activity of the western inner ring fault. (f) Volcano-tectonic collapse following AMS eruption controlling the deposition of the transgressive Pozzuoli Unit. Map inset also shows the activity of the western inner ring fault (g) Epoch3b renewed uplift with lava dome emplacement near the deformation centre and peripheral eruptions. Map inset also shows the activity of the western inner ring fault system. (h) Uplift centred in Pozzuoli and Monte Nuovo eruption at the periphery of the resurgent dome. Map inset also shows the activity of the western inner ring fault. Abbreviations: PPB: Penta Palummo Bank; M0: marine and volcaniclastic units older than CI; CI: Campanian Ignimbrite. M1: marine and volcaniclastic units younger than CI; NYT: Neapolitan Yellow Tuff; BA: Bacoli; PM: Porto Miseno; NB: Nisida Bank; ST: Santa Teresa; B-FdB: Baia-Fondi di Baia; CM: Capo Miseno; NI: Nisida; MN: Monte Nuovo. (For interpretation of the references to colour in this figure legend, the reader is referred to the Web version of this article.)

The southwestern portion of the IRFS and the southern part of the MRFS show discrete reactivation. Following this event, the caldera experienced subsidence with the deposition of the transgressive Pozzuoli Unit (4.44 ka, Isaia et al., 2009).

5.3.7. *Stage7: Epoch 3b uplift*

Renewed ground uplift, accompanied by seismo-volcanic activity, as documented by paleoliquefaction evidence (Vitale et al., 2019, 2022), predates the volcanic eruptions of Epoch 3b, with multiple dome intrusions in the central area and the last eruptions (i.e., Nisida, Capo Miseno; Smith et al., 2011) clustered along the ring faults (Fig. 8g). The western IRFS cross-cuts the sequences of this stage suggesting a mutual relationship between the doming and the activity of this fault system (Fig. 6a).

5.3.8. *Stage8: Monte Nuovo eruption*

After more than two millennia of quiescence, two-centuries-long volcano-tectonic crises ended with the eruption of Monte Nuovo in

1538 CE, again located close to the ring fault zone (Fig. 8h), following a ground uplift at the caldera centre (Di Vito et al., 2016). The western IRFS cross-cuts the S10 unit associated with Monte Nuovo tephra (Fig. 6b), suggesting its long-lived activity in the last 10 kyr.

6. Conclusive remarks

This work provides a backdrop for the formation and evolution of the offshore surficial structure of the CF caldera. A detailed structural map of the Pozzuoli Gulf, encompassing one-third of the CF caldera, is provided, and the activity of different fault systems in the last 40 kyr is defined. Two main fault systems were distinguished: the caldera ring and resurgent dome faults. The analysis of the displacement along the ring faults for the CI and NYT units indicates the occurrence of the CI caldera before the NYT eruption.

For the first time, we reconstructed three distinct caldera rims and associated fault zones that accommodated the CI caldera collapse at 40 ka and the subsequent NYT collapse at 15 ka. These offshore structures join with the two corresponding rims recognised on land, bounding the structural highs of Monte di Procida and Baia to the west and Posillipo to the east. Volcanic eruptions during inter-caldera periods generally occurred across the ring faults, with the caldera depression providing the necessary accommodation space to host volcaniclastic deposits. The caldera collapse associated with the NYT eruption produced differential reactivation of the preexisting CI caldera faults. The offshore collapse was accommodated mainly by the two innermost rims, which continue on land in Coroglio to the east and Toiano to the west. In the last 15 kyr, the ring faults had a pivotal role in controlling the upward magma migration and localisation of several eruptive vents, magmatic dikes, and hydrothermal fluids, a phenomenon that continues to the present day. Finally, the observation that ring faults at the shallow level (i.e., first 300 m) show normal kinematics and generally are not vertical, with dip angles of 60–80°, questioning previous literature reconstructions.

In the central part of the gulf, we recognised two fault sets, the older shows NE-SW to NNE-SSW strike, and an E-W strike marks the younger. The former faults form a depressed area in the dome culmination that continues on land with the graben bounded by the two structural highs of Rione Terra and La Pietra/Accademia. We associate this structural depression with a gravitational collapse at the reservoir scale likely related to the AMS eruption that also produced a minor caldera on-land. The detailed characterisation of such fault arrays is crucial to correlate local anomalies in the deformation pattern to existing structures, consider the role of such densely-spaced faults in conveying fluids toward the seafloor, and better define the hydrothermal system in the offshore region of the resurgent dome.

Our study highlights the crucial role of the ring faults in accommodating the subsidence of the caldera collar and in focusing localisation of post-caldera deformation. Because ring faults control magma migration and ascent, they may represent a preferred site for future eruptions. Furthermore, these deep-seated, intensely fractured zones connect the shallow hydrothermal system to the surface; hence their detailed analysis may have valuable implications for volcano monitoring purposes and geothermal potential characterisation and exploitation.

Author contributions

Conceptualization: J.N., S.V.; Design: J.N., S.V.; Seismic data: M.S., L.S., V.S.; Analysis and Interpretation: J.N., S.V.; Writing – original draft and figures preparation: J.N., S.V.; Writing – review and editing: J.N., S. V., L.F., R.I., G.C., M.S.; Supervision: S.V.

Declaration of competing interest

The authors declare that they have no known competing financial interests or personal relationships that could have appeared to influence the work reported in this paper.

Data availability

Supplementary files are available at the link provided in the dedicated section of the manuscript

Acknowledgements

The authors declared no conflict of interest. The GeoB08 seismic dataset was acquired during the CAFE-7/3 expedition funded by the Italian Research Council through the CNR Ship time Programme (Oceanographic Cruise_CAFE_07); the seismic acquisition was supported by the German Research Foundation (DFG) within the ICDP Priority Programme (Grant No. SP296/30-1). Data processing was funded through the DFG's ICDP Priority Programme (Grant No. SP296/34-1; SP296/34-2). The Seistec seismic dataset was acquired by the Italian Research Council CNR-ISMAR in 2013 during Oceanographic cruises Seistec_13, in cooperation with the Eo¨tvo¨s University of Budapest. We are grateful to Eliis for providing Paleoscan seismic interpretation software package. The authors acknowledge the Editor Fabrizio Agosta for his suggestions and editorial handling and the two anonymous reviewers for their comments and suggestions that improved the work. This work was supported by the University of Naples Federico II in the framework of Jacopo Natale's PhD project. This article is based on one of the chapters of his doctoral dissertation, which has benefited from the comments of the referees Prof. Guido Giordano and Dr Giovanni Luca Cardello.

Appendix A. Supplementary data

Supplementary data to this article can be found online at https://doi.org/10.1016/j.jsg.2022.104723.

References

Acocella, V., 2007. Understanding caldera structure and development: an overview of analogue models compared to natural calderas. Earth Sci. Rev. 85 (3–4), 125–160.
Acocella, V., 2008. Activating and reactivating pairs of nested collapses during caldera-forming eruptions: Campi Flegrei (Italy). Geophys. Res. Lett. 35 (17).
Acocella, V., 2010. Evaluating fracture patterns within a resurgent caldera: Campi Flegrei, Italy. Bull. Volcanol. 72 (5), 623–638.
Acocella, V., Cifelli, F., Funiciello, R., 2000. Analogue models of collapse calderas and resurgent domes. J. Volcanol. Geoth. Res. 104 (1–4), 81–96.
Aiello, G., Marsella, E., Di Fiore, V., 2012. New seismo-stratigraphic and marine magnetic data of the Gulf of Pozzuoli (Naples Bay, Tyrrhenian sea, Italy): inferences for the tectonic and magmatic events of the Phlegrean Fields volcanic complex (Campania). Mar. Geophys. Res. 33 (2), 97–125.
Aiello, G., Giordano, L., Giordano, F., 2016. High-resolution seismic stratigraphy of the Gulf of Pozzuoli (Naples Bay) and relationships with submarine volcanic setting of the Phlegrean Fields volcanic complex. Rendiconti Lincei 27 (4), 775–801.
Aiello, G., Iorio, M., Molisso, F., Sacchi, M., 2020. Integrated morpho-bathymetric, seismic-stratigraphic, and sedimentological data on the Dohrn canyon (Naples Bay, Southern Tyrrhenian Sea): relationships with volcanism and tectonics. Geosciences 10 (8), 319.
Albert, P.G., Giaccio, B., Isaia, R., Costa, A., Niespolo, E.M., Nomade, S., Pereira, A., Renne, P.R., Hinchliffe, A., Mark, D.F., Brown, R.J., Smith, V.C., 2019. Evidence for a large-magnitude eruption from Campi Flegrei caldera (Italy) at 29 ka. Geology 47 (7), 595–599.
Amoruso, A., Crescentini, L., D'Antonio, M., Acocella, V., 2017. Thermally-assisted magma emplacement explains restless calderas. Sci. Rep. 7 (1), 1–9.
Barberi, F., Cassano, E., La Torre, P., Sbrana, A., 1991. Structural evolution of Campi Flegrei caldera in light of volcanological and geophysical data. J. Volcanol. Geoth. Res. 48 (1–2), 33–49.
Bell, A.F., La Femina, P.C., Ruiz, M., Amelung, F., Bagnardi, M., Bean, C.J., Bernard, B., Ebinger, C., Gleeson, M., Grannell, J., Hernandez, S., Higgins, M., Liorzou, C., Lundgren, P., Meier, N.J., Mollhoff, M., Oliva, S., Ruiz, A.G., Stock, M.J., 2021. Caldera resurgence during the 2018 eruption of Sierra Negra volcano, gal´apagos Islands. Nat. Commun. 12 (1), 1–9.
Bevilacqua, A., Isaia, R., Neri, A., Vitale, S., Aspinall, W.P., Bisson, M., Flandoli, F., Baxter, P.J., Bertagnini, A., Ongaro, T.E., Iannuzzi, E., Pistolesi, M., Rosi, M., 2015. Quantifying volcanic hazard at Campi Flegrei caldera (Italy) with uncertainty assessment: 1. Vent opening maps. J. Geophys. Res. Solid Earth 120 (4), 2309–2329.
Bevilacqua, A., Flandoli, F., Neri, A., Isaia, R., Vitale, S., 2016. Temporal models for the episodic volcanism of Campi Flegrei caldera (Italy) with uncertainty quantification. J. Geophys. Res. Solid Earth 121 (11), 7821–7845.
Bevilacqua, A., Neri, A., Bisson, M., Esposti Ongaro, T., Flandoli, F., Isaia, R., Rosi, M., Vitale, S., 2017. The effects of vent location, event scale, and time forecasts on

pyroclastic density current hazard maps at Campi Flegrei caldera (Italy). Front. Earth Sci. 5, 72.
Bevilacqua, A., Neri, A., De Martino, P., Isaia, R., Novellino, A., Tramparulo, F.D.A., Vitale, S., 2020. Radial interpolation of GPS and leveling data of ground deformation in a resurgent caldera: application to Campi Flegrei (Italy). J. Geodes. 94 (2), 1–27.
Bischoff, A., Planke, S., Holford, S., Nicol, A., 2021. Seismic geomorphology, architecture and stratigraphy of volcanoes buried in sedimentary basins. In: Volcanoes-Updates in Volcanology. IntechOpen.
Branney, M., Acocella, V., 2015. Calderas. In: The Encyclopedia of Volcanoes. Academic Press, pp. 299–315.
Calderoni, G., Russo, F., 1998. The geomorphological evolution of the outskirts of Naples during the Holocene: a case study of the Bagnoli-Fuorigrotta depression. Holocene 8 (5), 581–588.
Camanni, G., Roche, V., Childs, C., Manzocchi, T., Walsh, J., Conneally, J., Saqab, M.M., Delogkos, E., 2019. The three-dimensional geometry of relay zones within segmented normal faults. J. Struct. Geol. 129, 103895.
Capuano, P., Russo, G., Civetta, L., Orsi, G., D'Antonio, M., Moretti, R., 2013. The active portion of the Campi Flegrei caldera structure imaged by 3-D inversion of gravity data. G-cubed 14 (10), 4681–4697.
Cardellini, C., Chiodini, G., Frondini, F., Avino, R., Bagnato, E., Caliro, S., Lelli, M., Rosiello, A., 2017. Monitoring diffuse volcanic degassing during volcanic unrests: the case of Campi Flegrei (Italy). Sci. Rep. 7 (1), 1–15.
Carlino, S., Somma, R., Troise, C., De Natale, G., 2012. The geothermal exploration of Campanian volcanoes: historical review and future development. Renew. Sustain. Energy Rev. 16 (1), 1004–1030.
Carlino, S., Mirabile, M., Troise, C., Sacchi, M., Zeni, L., Minardo, A., Caccavale, M., Daranyi, V., De Natale, G., 2016. Distributed-temperature-sensing using optical methods: a first application in the offshore area of Campi Flegrei caldera (Southern Italy) for volcano monitoring. Rem. Sens. 8 (8), 674.
Cartwright, J., James, D., Bolton, A.L., 2003. The genesis of polygonal fault systems: a review. Geol. Soc, London, Special Publ. 216 (1), 223–243.
Charlton, D., Kilburn, C., Edwards, S., 2020. Volcanic unrest scenarios and impact assessment at Campi Flegrei caldera, Southern Italy. J. Appl. Volcanol. 9 (1), 1–26.
Chiodini, G., Caliro, S., De Martino, P., Avino, R., Gherardi, F., 2012. Early signals of new volcanic unrest at Campi Flegrei caldera? Insights from geochemical data and physical simulations. Geology 40 (10), 943–946.
Colantoni, P., Del Monte, M., Fabbri, A., Gallignani, P., Selli, R., Tomadin, L., 1972. Ricerche geologiche nel Golfo di Pozzuoli.
Cole, J.W., Milner, D.M., Spinks, K.D., 2005. Calderas and caldera structures: a review. Earth Sci. Rev. 69 (1–2), 1–26.
Corradino, M., Pepe, F., Sacchi, M., Solaro, G., Duarte, H., Ferranti, L., Zinno, I., 2021. Resurgent uplift at large calderas and relationship to caldera-forming faults and the magma reservoir: new insights from the Neapolitan Yellow Tuff caldera (Italy). J. Volcanol. Geoth. Res. 411, 107183.
Corrado, G., De Lorenzo, S., Mongelli, F., Tramacere, A., Zito, G., 1998. Surface heat flow density at the Phlegrean Fields caldera (Southern Italy). Geothermics 27 (4), 469–484.
Costa, A., Folch, A., Macedonio, G., Giaccio, B., Isaia, R., Smith, V.C., 2012. Quantifying volcanic ash dispersal and impact of the Campanian Ignimbrite super-eruption. Geophys. Res. Lett. 39 (10).
D'Auria, L., Giudicepietro, F., Aquino, I., Borriello, G., Del Gaudio, C., Lo Bascio, D., Martini, M., Ricciardi, G.P., Ricciolino, P., Ricco, C., 2011. Repeated fluid-transfer episodes as a mechanism for the recent dynamics of Campi Flegrei caldera (1989–2010). J. Geophys. Res. Solid Earth 116 (B4).
De Astis, G., Pappalardo, L., Piochi, M., 2004. Procida volcanic history: new insights into the evolution of the Phlegraean Volcanic District (Campania region, Italy). Bull. Volcanol. 66 (7), 622–641.
De Martino, P., Dolce, M., Brandi, G., Scarpato, G., Tammaro, U., 2021. The ground deformation history of the neapolitan volcanic area (Campi Flegrei caldera, somma–vesuvius volcano, and Ischia Island) from 20 Years of continuous GPS observations (2000–2019). Rem. Sens. 13 (14), 2725.
De Natale, G., Troise, C., Mark, D., Mormone, A., Piochi, M., Di Vito, M.A., Isaia, R., Carlino, S., Barra, D., Somma, R., 2016. The Campi Flegrei deep drilling project (CFDDP): new insight on caldera structure, evolution and hazard implications for the Naples area (southern Italy). G-cubed 17 (12), 4836–4847.
De Siena, L., Sammarco, C., Cornwell, D.G., La Rocca, M., Bianco, F., Zaccarelli, L., Nakahara, H., 2018. Ambient seismic noise image of the structurally controlled heat and fluid feeder pathway at Campi Flegrei caldera. Geophys. Res. Lett. 45 (13), 6428–6436.
De Vita, S., Orsi, G., Civetta, L., Caran'ente, A., D'Antonio, M., Deino, A., di Cesare, T., Di Vito, M.A., Fisher, R.V., Isaia, R., Marotta, E., Necco, A., Ort, M., Pappalardo, L., Piochi, M., Southon, J., 1999. The agnano–monte Spina eruption (4100 years BP) in the restless Campi Flegrei caldera (Italy). J. Volcanol. Geoth. Res. 91 (2–4), 269–301.
Deino, A.L., Orsi, G., de Vita, S., Piochi, M., 2004. The age of the Neapolitan Yellow Tuff caldera-forming eruption (Campi Flegrei caldera–Italy) assessed by 40Ar/39Ar dating method. J. Volcanol. Geoth. Res. 133 (1–4), 157–170.
Del Gaudio, C., Aquino, I., Ricciardi, G.P., Ricco, C., Scandone, R., 2010. Unrest episodes at Campi Flegrei: a reconstruction of vertical ground movements during 1905–2009. J. Volcanol. Geoth. Res. 195 (1), 48–56.
Di Girolamo, P., Ghiara, M.R., Lirer, L., Munno, R., Rolandi, G., Stanzione, D., 1984. Vulcanologia e petrologia dei Campi Flegrei. Bollettino Societa` Geologica Italiana, p. 123.
Di Lieto, B., Romano, P., Bilham, R., Scarpa, R., 2021. Aseismic strain episodes at Campi Flegrei caldera, Italy. Adv. Geosci. 52, 119–129.
Di Luccio, F., Pino, N.A., Piscini, A., Ventura, G., 2015. Significance of the 1982–2014 Campi Flegrei seismicity: preexisting structures, hydrothermal processes, and hazard assessment. Geophys. Res. Lett. 42 (18), 7498–7506.
Di Vito, M.A., Isaia, R., Orsi, G., Southon, J.D., De'Vita, S., d'Antonio, M., Pappalardo, L., Piochi, M., 1999. Volcanism and deformation since 12,000 years at the Campi Flegrei caldera (Italy). J. Volcanol. Geoth. Res. 91 (2–4), 221–246.
Di Vito, M.A., Acocella, V., Aiello, G., Barra, D., Battaglia, M., Carandente, A., Del Gaudio, C., de Vita, S., Riccardi, G.P., Ricco, C., Scandone, R., Terrasi, F., 2016. Magma transfer at Campi Flegrei caldera (Italy) before the 1538 AD eruption. Sci. Rep. 6 (1), 1–9.
Diamanti, R., Camanni, G., Natale, J., Vitale, S., 2022. A gravitational origin for volcano-tectonic faults in the Campi Flegrei caldera (southern Italy) inferred from detailed field observations. J. Struct. Geol. 161, 104671.
Ebrahimi, P., Guarino, A., Allocca, V., Caliro, S., Avino, R., Bagnato, E., Capecchiacci, F., Carandente, A., Minopoli, C., Santi, A., Albanese, S., 2022. Hierarchical clustering and compositional data analysis for interpreting groundwater hydrogeochemistry: the application to Campi Flegrei volcanic aquifer (south Italy). J. Geochem. Explor. 233, 106922.
EMODnet Bathymetry Consortium, 2018. EMODnet Digital Bathymetry (DTM 2018).
Florio, G., Fedi, M., Cella, F., Rapolla, A., 1999. The Campanian Plain and Phlegrean Fields: structural setting from potential field data. J. Volcanol. Geoth. Res. 91 (2–4), 361–379.
Forni, F., Petricca, E., Bachmann, O., Mollo, S., De Astis, G., Piochi, M., 2018. The role of magma mixing/mingling and cumulate melting in the Neapolitan Yellow Tuff caldera-forming eruption (Campi Flegrei, Southern Italy). Contrib. Mineral. Petrol. 173 (6), 1–18.
Fusi, N., Mirabile, L., Camerlenghi, A., Ranieri, G., 1991. Marine geophysical survey of the Gulf of Naples (Italy): relationship between submarine volcanic activity and sedimentation. Mem. Soc. Geol. It. 47, 95–114.
Galetto, F., Bagnardi, M., Acocella, V., Hooper, A., 2019. Noneruptive unrest at the Caldera of Alcedo Volcano (Gal´apagos Islands) revealed by InSAR data and geodetic modeling. J. Geophys. Res. Solid Earth 124 (4), 3365–3381.
Geyer, A., Martí, J., 2014. A short review of our current understanding of the development of ring faults during collapse caldera formation. Front. Earth Sci. 2, 22.
Giaccio, B., Isaia, R., Fedele, F.G., Di Canzio, E., Hoffecker, J., Ronchitelli, A., Sinitsyn, A. A., Anikovich, M., Lisitsyn, S.N., Popov, V.V., 2008. The campanian ignimbrite and codola tephra layers: two temporal/stratigraphic markers for the early upper palaeolithic in southern Italy and eastern europe. J. Volcanol. Geoth. Res. 177 (1), 208–226.
Giaccio, B., Hajdas, I., Isaia, R., Deino, A., Nomade, S., 2017. High-precision 14 C and 40 Ar/39 Ar dating of the Campanian Ignimbrite (Y-5) reconciles the time-scales of climatic-cultural processes at 40 ka. Sci. Rep. 7 (1), 1–10.
Giudicepietro, F., Chiodini, G., Avino, R., Brandi, G., Caliro, S., De Cesare, W., Galluzzo, D., Esposito, A., La Rocca, A., Lo Bascio, D., Obrizzo, F., Pinto, S., Ricci, T., Ricciolino, P., Siniscalchi, A., Tramelli, A., Vandemeulebrouck, J., Macedonio, G., 2021. Tracking episodes of seismicity and gas transport in Campi Flegrei caldera through seismic, geophysical, and geochemical measurements. Seismol Res. Lett. 92 (2A), 965–975.
Grohmann, C.H., Campanha, G.A., 2010. OpenStereo: open source, cross-platform software for structural geology analysis. AGU Fall Meeting abstracts 2010. IN31C-06.
Guidoboni, E., Ciuccarelli, C., 2011. The Campi Flegrei caldera: historical revision and new data on seismic crises, bradyseisms, the Monte Nuovo eruption and ensuing earthquakes (twelfth century 1582 AD). Bull. Volcanol. 73 (6), 655–677.
Hardy, S., 2011. Cover deformation above steep, basement normal faults: insights from 2D discrete element modeling. Mar. Petrol. Geol. 28 (5), 966–972.
Hardy, S., 2013. Propagation of blind normal faults to the surface in basaltic sequences: insights from 2D discrete element modelling. Mar. Petrol. Geol. 48, 149–159.
Isaia, R., Marianelli, P., Sbrana, A., 2009. Caldera unrest prior to intense volcanism in Campi Flegrei (Italy) at 4.0 ka BP: implications for caldera dynamics and future eruptive scenarios. Geophys. Res. Lett. 36 (21).
Isaia, R., Vitale, S., Di Giuseppe, M.G., Iannuzzi, E., D'Assisi Tramparulo, F., Troiano, A., 2015. Stratigraphy, structure, and volcano-tectonic evolution of Solfatara maar-diatreme (Campi Flegrei, Italy). Bulletin 127 (9–10), 1485–1504.
Isaia, R., Iannuzzi, E., Sbrana, A., Marianelli, P., 2018. Note Illustrative Della Carta Geologica d'Italia Alla Scala 1: 50.000. Foglio 446-447 Napoli (aree emerse).
Isaia, R., Vitale, S., Marturano, A., Aiello, G., Barra, D., Ciarcia, S., Iannuzzi, E., Tramparulo, F.D.A., 2019. High-resolution geological investigations to reconstruct the long-term ground movements in the last 15 kyr at Campi Flegrei caldera (southern Italy). J. Volcanol. Geoth. Res. 385, 143–158.
Isaia, R., Di Giuseppe, M.G., Natale, J., Tramparulo, F.D.A., Troiano, A., Vitale, S., 2021. Volcano-tectonic setting of the pisciarelli fumarole field, Campi Flegrei caldera, southern Italy: insights into fluid circulation patterns and hazard scenarios. Tectonics 40 (5), e2020TC006227.
Jasim, A., Whitaker, F.F., Rust, A.C., 2015. Impact of channelized flow on temperature distribution and fluid flow in restless calderas: insight from Campi Flegrei caldera, Italy. J. Volcanol. Geoth. Res. 303, 157–174.
Judenherc, S., Zollo, A., 2004. The Bay of Naples (southern Italy): constraints on the volcanic structures inferred from a dense seismic survey. J. Geophys. Res. Solid Earth 109 (B10).
Marino, C., Ferranti, L., Natale, J., Anzidei, M., Benini, A., Sacchi, M., 2022. Quantitative reconstruction of Holocene ground displacements in the offshore part of the Campi Flegrei caldera (southern Italy): perspectives from seismo-stratigraphic and archaeological data. Mar. Geol. 447, 106797.
Milia, A., 1998. Stratigrafia, strutture deformative e considerazioni sull'origine delle unita` deposizionali oloceniche del Golfo di Pozzuoli (Napoli). Bollettino Societ`a Geologica Italiana 117, 777–787.

Milia, A., 2010. The stratigraphic signature of volcanism off Campi Flegrei (bay of Naples, Italy). GSA (Geol. Soc. Am.) Spec. Pap. (Reg. Stud.) 464, 155–170.
Milia, A., Torrente, M.M., Giordano, F., 2000. Active deformation and volcanism offshore Campi Flegrei, Italy: new data from high-resolution seismic reflection profiles. Mar. Geol. 171 (1–4), 61–73.
Monaco, L., Palladino, D.M., Albert, P.G., Arienzo, I., Conticelli, S., Di Vito, M., Fabbrizio, A., D'Antonio, M., Isaia, R., Manning, C.J., Nomade, S., Pereira, A., Petrosino, P., Sottili, G., Sulpizio, R., Zanchetta, G., Giaccio, B., 2022. Linking the Mediterranean MIS 5 tephra markers to Campi Flegrei (southern Italy) 109–92 ka explosive activity and refining the chronology of MIS 5c-d millennial-scale climate variability. Global Planet. Change 211, 103785.
Mosher, D.C., Simpkin, P.G., 1999. Status and trends of marine high-resolution seismic reflection profiling: data acquisition. Geosci. Can. 26, 174–188.
Natale, J., Ferranti, L., Marino, C., Sacchi, M., 2020. Resurgent dome faults in the offshore of the Campi Flegrei caldera (Pozzuoli Bay, Campania): preliminary results from high-resolution seismic reflection profiles. Boll. Geofis. Teor. Appl. 61 (3), 333–342.
Natale, J., Ferranti, L., Isaia, R., Marino, C., Sacchi, M., Spiess, V., Steinmann, L., Vitale, S., 2022. Integrated on-land-offshore stratigraphy of the Campi Flegrei caldera: new insights into the volcano-tectonic evolution in the last 15 kyr. Basin Res. 34 (2), 855–882.
Neri, A., Bevilacqua, A., Esposti Ongaro, T., Isaia, R., Aspinall, W.P., Bisson, M., Flandoli, F., Baxter, P.J., Bertagnini, A., Iannuzzi, E., Orsucci, S., Pistolesi, M., Rosi, M., Vitale, S., 2015. Quantifying volcanic hazard at Campi Flegrei caldera (Italy) with uncertainty assessment: 2. Pyroclastic density current invasion maps. J. Geophys. Res. Solid Earth 120 (4), 2330–2349.
Newhall, C.G., Dzurisin, D., 1988. Historical Unrest at the Large Calderas of the World (No. 1855). Department of the Interior, US Geological Survey.
Orsi, G., D'Antonio, M., de Vita, S., Gallo, G., 1992. The Neapolitan Yellow Tuff, a large-magnitude trachytic phreatoplinian eruption: eruptive dynamics, magma withdrawal and caldera collapse. J. Volcanol. Geoth. Res. 53 (1–4), 275–287.
Orsi, G., De Vita, S., Di Vito, M., 1996. The restless, resurgent Campi Flegrei nested caldera (Italy): constraints on its evolution and configuration. J. Volcanol. Geoth. Res. 74 (3–4), 179–214.
Orsi, G., Civetta, L., Del Gaudio, C., De Vita, S., Di Vito, M.A., Isaia, R., Petrazzuoli, S.M., Ricciardi, G.P., Ricco, C., 1999. Short-term ground deformations and seismicity in the resurgent Campi Flegrei caldera (Italy): an example of active block-resurgence in a densely populated area. J. Volcanol. Geoth. Res. 91 (2–4), 415–451.
Orsi, G., Di Vito, M.A., Isaia, R., 2004. Volcanic hazard assessment at the restless Campi Flegrei caldera. Bull. Volcanol. 66 (6), 514–530.
Paleoscan, Eliis, 2018. https://www.eliis-geo.com/.
Pappalardo, L., Civetta, L., d'Antonio, M., Deino, A., Di Vito, M., Orsi, G., Carandente, A., de Vita, S., Isaia, R., Piochi, M., 1999. Chemical and Sr-isotopical evolution of the phlegraean magmatic system before the campanian ignimbrite and the neapolitan Yellow tuff eruptions. J. Volcanol. Geoth. Res. 91 (2–4), 141–166.
Pepe, S., De Siena, L., Barone, A., Castaldo, R., D'Auria, L., Manzo, M., Casu, F., Fedi, M., Lanari, R., Bianco, F., Tizzani, P., 2019. Volcanic structures investigation through SAR and seismic interferometric methods: the 2011–2013 Campi Flegrei unrest episode. Rem. Sens. Environ. 234, 111440.
Perrotta, A., Scarpati, C., Luongo, G., Morra, V., 2006. The Campi Flegrei caldera boundary in the city of Naples. Develop. Volcanol. 9, 85–96 (Elsevier).
Pescatore, T., Diplomatico, G., Senatore, M., Tramutoli, M., Mirabile, L., 1984. Contributi allo studio del Golfo di Pozzuoli: Aspetti stratigrafici e strutturali.
Petrosino, P., Arienzo, I., Mazzeo, F.C., Natale, J., Petrelli, M., Perugini, D., D'Antonio, M., 2019. The San Gregorio Magno lacustrine basin (Campania, southern Italy): improved characterization of the tephrostratigraphic markers based on trace elements and isotopic data. J. Quat. Sci. 34, 393–404.
Reiter, F., Acs, P., 1996-2020. TectonicsFP ©1996-2020 Help Version 1.7.14, 2020-02-02.
Robertson, R.M., Kilburn, C.R., 2016. Deformation regime and long-term precursors to eruption at large calderas: Rabaul, Papua New Guinea. Earth Planet Sci. Lett. 438, 86–94.
Roche, V., Camanni, G., Childs, C., Manzocchi, T., Walsh, J., Conneally, J., Saqab, M.M., Delogkos, E., 2021. Variability in the three-dimensional geometry of segmented normal fault surfaces. Earth Sci. Rev. 216, 103523.
Roche, O., Druitt, T.H., 2001. Onset of caldera collapse during ignimbrite eruptions. Earth Planet Sci. Lett. 191, 191–202.
Rolandi, G., Bellucci, F., Heizler, M.T., Belkin, H.E., De Vivo, B., 2003. Tectonic controls on the genesis of ignimbrites from the Campanian Volcanic Zone, southern Italy. Mineral. Petrol. 79 (1), 3–31.
Rolandi, G., Di Lascio, M., Rolandi, R., 2020. The neapolitan Yellow tuff eruption as the source of the Campi Flegrei caldera. In: Vesuvius, Campi Flegrei, and Campanian Volcanism. Elsevier, pp. 273–296.
Rosi, M., Sbrana, A., 1987. Phlegrean fields. Quad. La Ric. Sci. 9 (114).
Rosi, M., Sbrana, A., Principe, C., 1983. The Phlegraean Fields: structural evolution, volcanic history and eruptive mechanisms. J. Volcanol. Geoth. Res. 17 (1–4), 273–288.
Ruch, J., Acocella, V., Geshi, N., Nobile, A., Corbi, F., 2012. Kinematic analysis of vertical collapse on volcanoes using experimental models time series. J. Geophys. Res. Solid Earth 117 (B7).
Sacchi, M., Alessio, G., Aquino, I., Esposito, E., Molisso, F., Nappi, R., Porfido, S., Violante, C., 2009. Preliminary results of the oceanographic cruise CAFE_07 – leg 3 in the bays of napoli and Pozzuoli, eastern Tyrrhenian Sea. Quaderni Geofisc. 64, 3–26.
Sacchi, M., Pepe, F., Corradino, M., Insinga, D.D., Molisso, F., Lubritto, C., 2014. The Neapolitan Yellow Tuff caldera offshore the Campi Flegrei: stratal architecture and kinematic reconstruction during the last 15 ky. Mar. Geol. 354, 15–33.
Sacchi, M., Caccavale, M., Corradino, M., Esposito, G., Ferranti, L., Ha´mori, Z., Horvath, F., Insinga, D., Marino, C., Matano, F., Molisso, F., Natale, J., Passaro, S., Pepe, F., To´th, T., 2019. The use and beauty of ultra-high-resolution seismic reflection imaging in Late Quaternary marine volcaniclastic settings, Napoli Bay, Italy. Foldtani Kozlony 149 (3, 4), 371.
Sacchi, M., Passaro, S., Molisso, F., Matano, F., Steinmann, L., Spiess, V., Pepe, F., Corradino, M., Caccavale, M., Tamburrino, S., Esposito, G., Vallefuoco, M., Ventura, G., 2020. The holocene marine record of unrest, volcanism, and hydrothermal activity of Campi Flegrei and Somma–Vesuvius. In: Vesuvius, Campi Flegrei, and Campanian Volcanism. Elsevier, pp. 435–469.
Sbrana, A., Marianelli, P., Pasquini, G., 2021. The phlegrean fields volcanological evolution. J. Maps 17 (2), 557–570.
Scarpati, C., Perrotta, A., 2016. Stratigraphy and physical parameters of the Plinian phase of the Campanian Ignimbrite eruption. Bulletin 128 (7–8), 1147–1159.
Scarpati, C., Cole, P., Perrotta, A., 1993. The Neapolitan Yellow Tuff—a large volume multiphase eruption from Campi Flegrei, southern Italy. Bull. Volcanol. 55 (5), 343–356.
Scarpati, C., Perrotta, A., Lepore, S., Calvert, A., 2013. Eruptive history of Neapolitan volcanoes: constraints from 40Ar–39Ar dating. Geol. Mag. 150 (3), 412–425.
Scarpati, C., Sparice, D., Perrotta, A., 2020. Dynamics of large pyroclastic currents inferred by the internal architecture of the Campanian Ignimbrite. Sci. Rep. 10 (1), 1–13.
Secomandi, M., Paoletti, V., Aiello, G., Fedi, M., Marsella, E., Ruggieri, S., D'Argenio, B., Rapolla, A., 2003. Analysis of the magnetic anomaly field of the volcanic district of the Bay of Naples, Italy. Mar. Geophys. Res. 24 (3), 207–221.
Selva, J., Orsi, G., Di Vito, M.A., Marzocchi, W., Sandri, L., 2012. Probability hazard map for future vent opening at the Campi Flegrei caldera, Italy. Bull. Volcanol. 74 (2), 497–510.
Silleni, A., Giordano, G., Isaia, R., Ort, M.H., 2020. The Magnitude of the 39.8 Ka Campanian Ignimbrite Eruption, Italy: Method, Uncertainties and Errors. Field Data, Models and Uncertainty in Hazard Assessment of Pyroclastic Density Currents and Lahars: Global Perspectives.
Simpkin, P.G., Davis, A., 1993. For seismic profiling in very shallow water, a novel receiver. Sea Technol. 34, 21–28.
Siniscalchi, A., Tripaldi, S., Romano, G., Chiodini, G., Improta, L., Petrillo, Z., D'Auria, L., Caliro, S., Avino, R., 2019. Reservoir structure and hydraulic properties of the Campi Flegrei geothermal system inferred by audiomagnetotelluric, geochemical, and seismicity study. J. Geophys. Res. Solid Earth 124 (6), 5336–5356.
Smith, V.C., Isaia, R., Pearce, N.J.G., 2011. Tephrostratigraphy and glass compositions of post-15 kyr Campi Flegrei eruptions: implications for eruption history and chronostratigraphic markers. Quat. Sci. Rev. 30 (25–26), 3638–3660.
Somma, R., Iuliano, S., Matano, F., Molisso, F., Passaro, S., Sacchi, M., Troise, C., De Natale, G., 2016. High-resolution morpho-bathymetry of Pozzuoli bay, southern Italy. J. Maps 12 (2), 222–230.
Sparks, R.S.J., Biggs, J., Neuberg, J.W., 2012. Monitoring volcanoes. Science 335 (6074), 1310–1311.
Steinmann, L., Spiess, V., Sacchi, M., 2016. The Campi Flegrei caldera (Italy): formation and evolution in interplay with sea-level variations since the Campanian Ignimbrite eruption at 39 ka. J. Volcanol. Geoth. Res. 327, 361–374.
Steinmann, L., Spiess, V., Sacchi, M., 2018. Post-collapse evolution of a coastal caldera system: insights from a 3D multichannel seismic survey from the Campi Flegrei caldera (Italy). J. Volcanol. Geoth. Res. 349, 83–98.
Tibaldi, A., Pasquare, F.A., Papanikolaou, D., Nomikou, P., 2008. Tectonics of Nisyros Island, Greece, by field and offshore data, and analogue modelling. J. Struct. Geol. 30 (12), 1489–1506.
Torrente, M.M., Milia, A., 2018. Comment on "The Campi Flegrei Deep Drilling Project (CFDDP): new insight on caldera structure, evolution and hazard implications for the Naples area (Southern Italy)" by G. De Natale et al. G-cubed 19 (7), 2283–2288.
Torrente, M.M., Milia, A., Bellucci, F., Rolandi, G., 2010. Extensional tectonics in the Campania Volcanic Zone (eastern Tyrrhenian Sea, Italy): new insights into the relationship between faulting and ignimbrite eruptions. Italian J. Geosci. 129 (2), 297–315.
Tramelli, A., Giudicepietro, F., Ricciolino, P., Chiodini, G., 2022. The seismicity of Campi Flegrei in the contest of an evolving long term unrest. Sci. Rep. 12, 2009.
Troiano, A., Isaia, R., Di Giuseppe, M.G., Tramparulo, F.D.A., Vitale, S., 2019. Deep electrical resistivity tomography for a 3D picture of the most active sector of Campi Flegrei caldera. Sci. Rep. 9 (1), 1–10.
Vanorio, T., Virieux, J., Capuano, P., Russo, G., et al., 2005. Three-dimensional seismic tomography from P wave and S wave microearthquake travel times and rock physics characterization of the Campi Flegrei Caldera. J. Geophys. Res.: Solid Earth 110 (B3).
Vitale, S., Ciarcia, S., 2013. Tectono-stratigraphic and kinematic evolution of the southern Apennines/Calabria–Peloritani Terrane system (Italy). Tectonophysics 583, 164–182.
Vitale, S., Ciarcia, S., 2018. Tectono-stratigraphic setting of the Campania region (southern Italy). J. Maps 14 (2), 9–21.
Vitale, S., Isaia, R., 2014. Fractures and faults in volcanic rocks (Campi Flegrei, southern Italy): insight into volcano-tectonic processes. Int. J. Earth Sci. 103 (3), 801–819.
Vitale, S., Isaia, R., Ciarcia, S., Di Giuseppe, M.G., Iannuzzi, E., Prinzi, E.P., Tramparulo, F.D.A., Troiano, A., 2019. Seismically induced soft-sediment deformation phenomena during the volcano-tectonic activity of Campi Flegrei caldera (southern Italy) in the last 15 kyr. Tectonics 38 (6), 1999–2018.

Vitale, S., Prinzi, E.P., Tramparulo, F.D.A., De Paola, C., Di Maio, R., Piegari, E., Sabbatino, M., Natale, J., Notaro, P., Ciarcia, S., 2020. Late miocene-early pliocene out-of-sequence thrusting in the southern apennines (Italy). Geosciences 10 (8), 301.
Vitale, S., Natale, J., Isaia, R., Tramparulo, F.D.A., Ciarcia, S., 2022. Evidence of seismic-related liquefaction processes within the volcanic record of the Campi Flegrei caldera (Italy). Geosciences 12, 241.
Walter, T.R., 2008. Facilitating dike intrusions into ring-faults. Develop. Volcanol. 10, 351–374.
Wohletz, K., Orsi, G., De Vita, S., 1995. Eruptive mechanisms of the Neapolitan Yellow Tuff interpreted from stratigraphie, chemical, and granulometric data. J. Volcanol. Geoth. Res. 67 (4), 263–290.
Young, N., Isaia, R., Gottsmann, J., 2020. Gravimetric constraints on the hydrothermal system of the Campi Flegrei caldera. J. Geophys. Res. Solid Earth 125 (7), e2019JB019231.
Zollo, A., Judenherc, S., Auger, E., D'Auria, L., Virieux, J., Capuano, P., Chiarabba, C., de Franco, R., Makris, J., Michelini, A., Musacchio, G., 2003. Evidence for the buried rim of Campi Flegrei caldera from 3-d active seismic imaging. Geophys. Res. Lett. 30 (19).